Review

Tip of the Iceberg: A New Wave of Iron–Sulfur Cluster Proteins Found in Viruses

Audrey L. Heffner [1,2] and Nunziata Maio [1,*]

1   Molecular Medicine Branch, *Eunice Kennedy Shriver* National Institute of Child Health and Human Development, Bethesda, MD 20892, USA; audrey.heffner@nih.gov
2   Department of Biology, Johns Hopkins University, Baltimore, MD 21218, USA
*   Correspondence: maion@mail.nih.gov

Abstract: Viruses rely on host cells to replicate their genomes and assemble new viral particles. Thus, they have evolved intricate mechanisms to exploit host factors. Host cells, in turn, have developed strategies to inhibit viruses, resulting in a nuanced interplay of co-evolution between virus and host. This dynamic often involves competition for resources crucial for both host cell survival and virus replication. Iron and iron-containing cofactors, including iron–sulfur clusters, are known to be a heavily fought for resource during bacterial infections, where control over iron can tug the war in favor of the pathogen or the host. It is logical to assume that viruses also engage in this competition. Surprisingly, our knowledge about how viruses utilize iron (Fe) and iron–sulfur (FeS) clusters remains limited. The handful of reviews on this topic primarily emphasize the significance of iron in supporting the host immune response against viral infections. The aim of this review, however, is to organize our current understanding of how viral proteins utilize FeS clusters, to give perspectives on what questions to ask next and to propose important avenues for future investigations.

Keywords: iron–sulfur cluster biogenesis; HSC20 (aka HSCB); HSPA9; cytoplasmic iron–sulfur cluster assembly; CIAO1; MMS19; FAM96B; COVID-19; viral proteins; viral replication

1. Iron–Sulfur Clusters as Essential Cofactors in Cells from Bacteria to Humans

Virtually every cell on Earth ingeniously harnesses FeS clusters as crucial cofactors in a multitude of biological processes [1,2]. FeS enzymes are integral to mitochondrial respiration [3], the TCA cycle [4], nitrogen fixation [5], DNA replication and repair [6–9], protein translation [10], heme and cofactor biosynthesis [11–13], and sensing and regulation of iron levels [4,14,15], among others. FeS clusters play both structural and functional roles by acting in electron transfer processes, oxidoreductive reactions, and protein conformational changes—an ability not inherently shared by other metal ions [2,16,17]. It is likely that iron–sulfur clusters are utilized to a greater extent than our current observation suggests. These cofactors are prone to oxidative destabilization in oxygen-rich environments, such as those encountered during purification processes [1,16,18]. While atmospheric oxygen levels hover at approximately 21 percent, the interior of a mammalian cell typically ranges between 0.5 and 5 percent [19,20].

As a result, handling of FeS proteins following lysis of the cell requires special tools and protocols. Additionally, the characterization of FeS proteins necessitates the use of sophisticated techniques. In conjunction with modeling studies and, more recently, bioinformatics approaches, these methods contribute to a holistic understanding of this class of inorganic cofactors, representing a fundamental aspect of bioinorganic chemistry. UV–vis absorption, Mössbauer and electron paramagnetic resonance (EPR) spectroscopies remain the most commonly used and robust methods for unraveling optical properties, electronic configurations, oxidation states and coordination environments of FeS clusters [21].

Nuclear magnetic resonance (NMR), electron-nuclear double resonance (ENDOR) and Raman spectroscopies have also found application in the study of FeS proteins [22]. More

recently, native mass spectrometry (MS) and time-resolved native MS have emerged as powerful tools, providing detailed and unambiguous information about the type of cluster coordinated by a protein and the coordinating amino acid residues [23].

While our manuscript primarily focuses on viral genomes that encode FeS proteins, we acknowledge the essential contributions of spectroscopic, modeling, and bioinformatics approaches to the characterization of the structure and function of FeS proteins. These multifaceted methodologies have played a crucial role in advancing our understanding of the complex nature of FeS clusters, establishing them as indispensable tools in the field of bioinorganic chemistry.

FeS proteins are not only ubiquitous, but the roles performed by FeS clusters have remained remarkably conserved throughout evolution (Figure 1C) [24]. Depending on the organism, the bacterial NADH dehydrogenase complex contains seven to ten FeS clusters conserved in the eukaryotic mitochondrial respiratory complex I which typically ligates eight clusters [3,25]. Electron transfer between FeS clusters in complex I is coupled to proton pumping across the mitochondrial inner membrane, accounting for approximately 40% of the total protons pumped throughout the respiratory chain [3,25]. DNA replication proteins, including DNA polymerase-α, DNA polymerase-δ, DNA polymerase-ε, DNA primase, and DNA repair nucleases—NTHL1 and MUTYH—rely on iron–sulfur clusters for their imperative function in supporting genome maintenance and cell proliferation (Figure 1C) [6–9,26].

Cells have evolved intricate biosynthetic pathways to assemble FeS clusters and incorporate them into a vast array of proteins. De novo biogenesis of FeS clusters is a complex multistep process highly conserved from bacteria to humans [24,27,28]. In mammalian cells, the basic building block of all FeS clusters, the rhombic [2Fe-2S] cluster, is initially assembled on a main scaffold protein, ISCU [24,27,29–34]. ISCU binds to a dimeric configuration of the cysteine desulfurase, NFS1, which enzymatically converts cysteine to alanine, while mobilizing inorganic sulfur for FeS cluster assembly [24,27,29,30,35]. Specifically, in the catalytic reaction carried out by NFS1, sulfur from the thiol group of the substrate cysteine is mobilized to generate a persulfide intermediate on cysteine 138 of ISCU [31]. NFS1 is stabilized by its essential binding partner ISD11 [36–38]. The identity of the iron donor for FeS cluster assembly in mitochondria remains controversial in the field. In the cytosol, PCBP1 and its binding partner, BOLA2, have been found to provide iron for [2Fe-2S] cluster assembly [39]. PCBP1 can coordinate up to three ferrous iron ions and has been shown to function as a chaperone that delivers iron to the storage protein ferritin as well as to other cytosolic iron proteins [40–43]. Additionally, two electrons are needed for [2Fe-2S] cluster assembly. In yeast and mitochondria, these reducing equivalents are provided by the ferredoxin/ferredoxin reductase complex [44,45]. The [2Fe-2S] cluster can then be utilized to generate much more complex FeS cofactors with different stoichiometries of iron and sulfur, including the most common cubane [4Fe-4S] clusters (Figure 1A) [1,46]. FeS clusters of more complex structures can be assembled on secondary carriers which in turn deliver the cofactors to subsets of recipient FeS proteins [24]. Cubane [4Fe-4S] clusters can be generated by the reductive coupling of two [2Fe-2S] clusters [46]. and are commonly found in DNA and RNA enzymes where changes in the oxidation state of [4Fe-4S] clusters have been proposed to modulate affinity of binding to the DNA or RNA polyanion [6–9,47]. Cubane clusters function in complex electron relay systems where they allow facile electron transfer that is not coupled to changes in the conformation of the cluster due to the delocalization of electrons between iron atoms [1,21].

Transfer of newly assembled FeS clusters to recipient apo-proteins is assisted and enhanced by an evolutionarily conserved chaperone/co-chaperone system [48–51]. In humans, the ATP-dependent Hsp70 chaperone, HSPA9, and its cognate J-domain protein, HSC20 (or HSCB), facilitate transfer of FeS clusters to recipient proteins (Figure 1B) [30,50,52]. The selection process for specifically allocating FeS clusters to only FeS apoproteins among the entire proteome has represented a long-standing question in the field. One mechanism has emerged in recent years that focuses on the specificity driven by the co-chaperone,

HSC20, given that the multifunctional chaperone HSPA9 has promiscuous substrate-binding activity [51,53,54]. HSC20 was found to recognize Leucine-Tyrosine-Arginine (LYR)-like motifs present in recipient FeS apo-proteins for direct binding and delivery of a FeS cluster [30,50,52]. The C-terminal domain of HSC20 interacts directly with the FeS-bound ISCU, which is released from the initial pre-complex with NFS1, and a histidine–proline–aspartate (HPD) tripeptide in the N-terminal J-domain of HSC20 activates the ATP hydrolysis by HSPA9, thereby accelerating cluster transfer [30,50,52,55–57]. Once transferred to the appropriate recipients, the current understanding is that the protein folds around the FeS cluster [58]. A subset of nucleocytoplasmic FeS proteins, such as those involved in DNA replication and repair, purine and pyrimidine metabolism and tRNA modifications, require the specialized Cytoplasmic Iron–sulfur Assembly (CIA) complex to acquire their cofactors (Figure 1B) [59–62]. The CIA complex is composed of MMS19, CIAO1, and FAM96B [59–61]. MMS19 is essential for genome stability and DNA metabolism [59,60] and possesses four HEAT repeat motifs that have been proposed to mimic the DNA double helix, which could provide an appropriate docking site for DNA or RNA binding proteins [63]. Binding of HSC20 to the LYR motif of CIAO1 likely bridges the CIA machinery to the de novo FeS complex [61]. A model has been proposed, whereby a dimer of HSC20 engages simultaneously the LYR motif of CIAO1 that is bound to MMS19 and FAM96B, and the LYR sequence of an unfolded FeS-recipient apoprotein, thereby mediating the interaction of the FeS client with the CIA complex and facilitating cluster acquisition [24,61]. Overall, the relevance of the FeS biogenesis pathway for human health and disease has become particularly apparent during the past twenty years with the identification of several ultra-rare disorders caused by loss of function in the genes that encode the highly conserved FeS biogenesis proteins [24,27,64]. Interestingly, the physiological consequences of loss of function in any of the CIA machinery components have remained unknown until recently, when biallelic pathogenic variants in *CIAO1* were reported to result in a novel disorder characterized by predominantly neuromuscular manifestations [65]. CIAO1 deficiency also caused a multisystemic involvement that included neurobehavioral comorbidities and iron deposition in deep brain nuclei, underscoring the involvement of CIAO1, and by extension of the CIA machinery, in multiple metabolic pathways and physiological systems [65]. Exome sequencing has effectively contributed to uncover novel ultra-rare human conditions through the identification of genetic variants that have enabled a better understanding of disease mechanisms and the identification of potential targets for therapeutic interventions. It is likely that in the years to come, many more human conditions will emerge due to loss of function in components of the FeS biogenesis pathway, which have yet to be associated with any known human diseases.
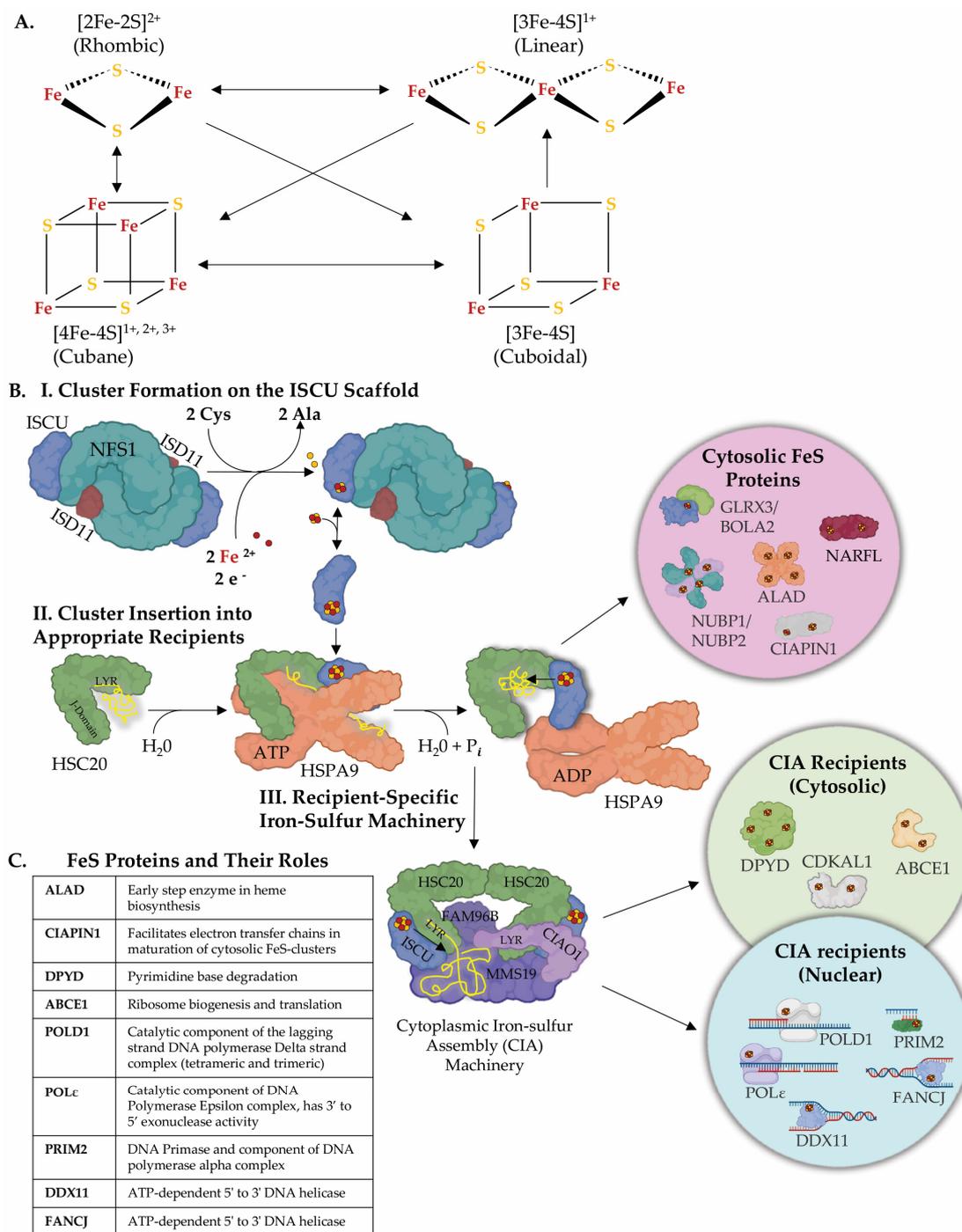
ALAD	Early step enzyme in heme biosynthesis
CIAPIN1	Facilitates electron transfer chains in maturation of cytosolic FeS-clusters
DPYD	Pyrimidine base degradation
ABCE1	Ribosome biogenesis and translation
POLD1	Catalytic component of the lagging strand DNA polymerase Delta strand complex (tetrameric and trimeric)
POLε	Catalytic component of DNA Polymerase Epsilon complex, has 3' to 5' exonuclease activity
PRIM2	DNA Primase and component of DNA polymerase alpha complex
DDX11	ATP-dependent 5' to 3' DNA helicase
FANCJ	ATP-dependent 5' to 3' DNA helicase

Figure 1. Iron–sulfur clusters and their assembly. (**A**) Biologically relevant FeS cluster geometries and possible interconversions [16]. (**B**) Iron sulfur cluster biogenesis is a complex highly regulated process that requires two basic steps: (I) de novo FeS cluster formation on the main scaffold ISCU [24,27,29,30] by the activity of a cysteine desulfurase, NFS1, which converts cysteine to alanine and generates a persulfide intermediate on ISCU in the process [24,27,29,30]. Donation of iron and reducing equivalents completes [2Fe-2S] cluster assembly on the main scaffold ISCU [39]. (II) The newly assembled FeS cluster is delivered to the appropriate recipient proteins by the activity of an HSP70 chaperone and cognate J-domain HSP40 cochaperone system [30,50,52]. In mammalian cells, the chaperone is HSPA9 and the cochaperone HSC20 (aka HSCB). HSC20 recognizes LYR-like motifs present in subsets of FeS recipient proteins [30,50,52]. In the cytosol of mammalian cells, following cluster incorporation, a subset of proteins, such as NARFL and CIAPIN1, complete their maturation

and become active [30,50,52]. (III) Nucleic acid processing enzymes require a highly specialized cytoplasmic iron–sulfur assembly (CIA) complex to acquire their cofactors [30,61]. The CIA complex consists of CIAO1, MMS19, and FAM96B. CIAO1 was found to harbor a highly conserved LYR-motif that engages the cochaperone HSC20, thereby acting as a bridge between CIA and the de novo FeS assembly machinery [30,61]. A subset of FeS proteins that acquire their cofactors from the CIA complex, (e.g., DPYD and ABCE1) may function in the cytosol, while others are translocated to the nucleus (POLD1, PRIM2, FANCJ) [7]. (**C**) Representative FeS proteins with their roles discussed. Examples of well-known FeS proteins are listed. In each case, their distinctive roles are highlighted. The diverse functions range from electron transfer to catalytic processes, showcasing the versatility of FeS clusters in various essential biological contexts. Panel (**B**) created with the help of BioRender.com.

2. Viral Genome Evolution: Harnessing the Host Machinery and FeS Clusters

Unlike bacterial pathogens, many viruses evolved as genetic minimalists to evade host targeting strategies raised against their viral genomes [66,67]. Capsids and nucleocapsids also limit genome lengths and require the genome to squeeze into small protein capids [66,68]. To overcome these feats, many viruses have evolved complicated genomes with intricate replication and transcription mechanisms. Even the larger DNA viruses, which can be larger than the genomes of the smallest bacterium, do not encode all the necessary components for the production of progeny [69,70]. Instead of incorporating all of the necessary components into their minimalist genomes, viruses smartly use the host cell machinery. This extends to their utilization of the host cell FeS cluster assembly machinery. Why invest time, energy, and genome space into something already encoded by every potential host? This review showcases five diverse virus families that have been reported to encode FeS proteins.

3. FeS Clusters in Virally Encoded Proteins of Five Distinct Virus Families

3.1. The Rotavirus Non-Structural Protein 5, NSP5

The initial discovery of a virally encoded FeS protein, the rotavirus NSP5, was likely serendipitous, recognized by the appearance of an unexpected brown color during the purification process, indicating its potential coordination of a FeS cluster [71]. The rotavirus non-structural protein 5, NSP5, has been reported to ligate a [2Fe-2S] cluster based on distinctive features observed on EPR spectroscopy [71]. Rotaviruses mainly infect enterocytes of the small intestine villi and can cause severe diarrhea, which can be deadly in infants and immunocompromised patients [72]. No specific treatments are available for rotavirus infections [72].

Rotaviruses contain eleven double-stranded RNA (dsRNA) segments inside three-layered proteinaceous virions or virus particles [73]. The total genome size is approximately 18 kilobases (kb), and each dsRNA segment is between 600 base pairs (bp) and 3300 bp [73]. Rotavirus NSP5 and NSP2 are responsible for forming liquid-like protein-RNA condensates that provide an appropriate environment for RNA replication, known as viroplasms (Figure 2) [73–75]. Never exposed to the cytoplasm, the dsRNA genome is transcribed and capped by VP1, the RNA-dependent RNA polymerase (RdRp), inside virions that have lost their outermost protein layer in the lysosomal lumen [73]. Transcription of the dsRNA segments by the RdRp generates positive (+) sense single-stranded RNAs (ssRNA) which are extruded from the virions to be either translated by the host cell ribosomes or to serve as templates for replication [73]. In the latter case, NSP2 binds the (+)ssRNAs in a sequence-specific manner and acts as an RNA chaperone by facilitating the folding of RNA into inter-segmented intermediates (Figure 2) [73]. Eleven single-stranded inter-segmented RNAs, NSP2 and NSP5, VP2 and VP1 form the inner core of a virion inside the viroplasms. Replication of (+)ssRNA templates occurs within these virion cores generating the dsRNA segments of the rotavirus genome [73]. NSP5 has been proposed to act as a scaffold linking replication and transcription of the (+)ssRNA by binding to VP1 and the core structure formed by VP2 [71,73,74]. The virion core is encased in the triple-protein outer layer [73].

There remain several unknowns in the current model of rotavirus replication, leaving much yet to be uncovered.
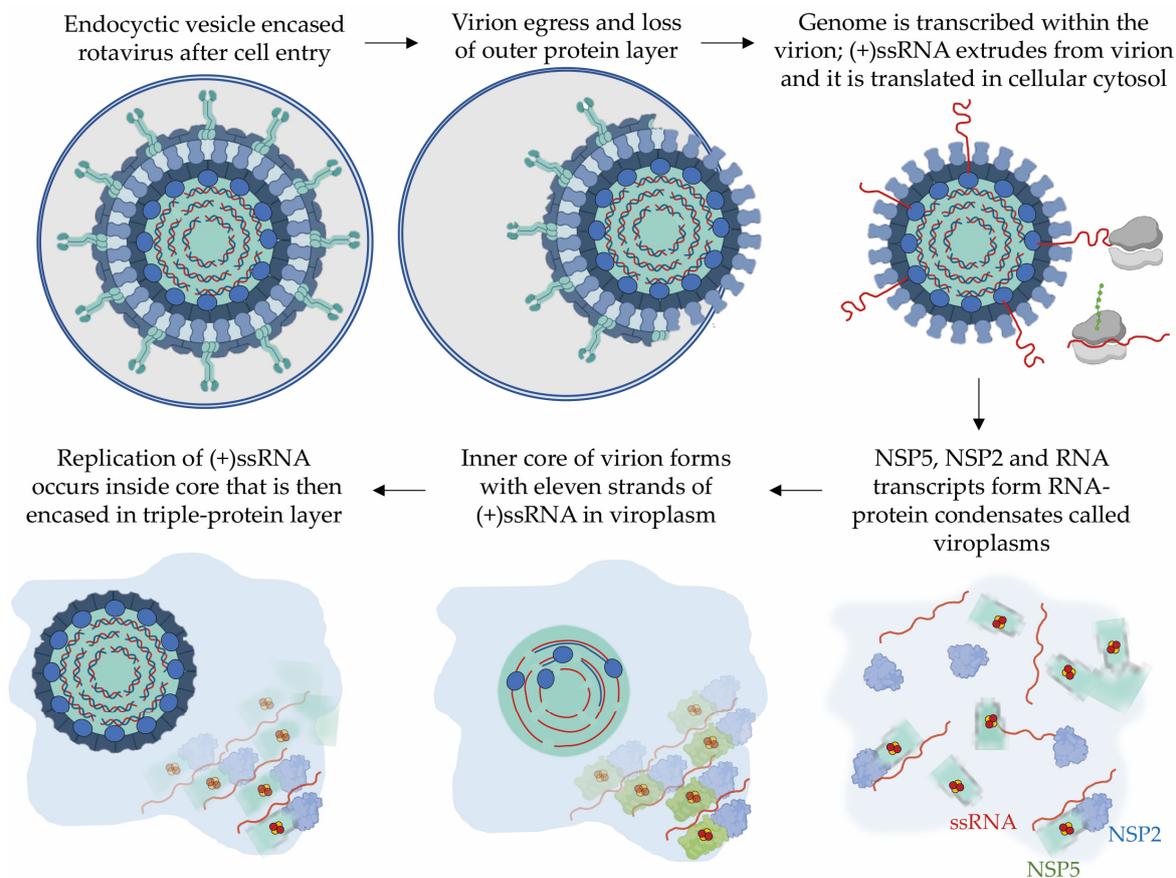

Figure 2. The rotavirus infection cycle and its NSP5. Upon entering the cell, the rotavirus undergoes a process whereby its outer layer of triple-protein encasement is shed, allowing the virion to be released from the vesicle [73]. Subsequently, within the cytosol, the double-stranded RNA (dsRNA) genome is transcribed by the polymerase VP1 while remaining confined within the virion, thereby preventing direct contact with the immune-ready cytosol [73]. Positive-sense single-stranded RNAs ((+)ssRNAs) are extruded from the virion and are either translated or serve as templates for the synthesis of new virion dsRNA [73]. This process involves NSP5 and NSP2. RNA transcripts forming RNA-protein condensates, known as viroplasms, serve as the location for the assembly of new virions [73]. Within viroplasms, the inner core of the virion is assembled, comprising eleven distinct strands of (+)ssRNA that act as templates for the dsRNA genome of the newly forming virion [73]. Replication of these templates occurs within the core, which is subsequently encapsulated with the triple-protein layer, completing the formation of new virions [73]. Figure created with the help of BioRender.com.

A recombinant rotavirus lacking NSP5 produced by reverse genetics was unable to form viroplasms and replicate viral RNA, while infection of a cell-line expressing wild-type NSP5 was able to rescue replication of the viral RNA [76]. NSP5 has an N-terminal intrinsically disordered region, two oligomerization domains, and an amphipathic alpha-helical C-terminus [74]. Additionally, NSP5 has been found to harbor ATPase activity [74], and phosphorylation of multiple serine residues has been reported to modulate NSP5 function [74,76].

Interestingly, aerobic purification of NSP5 resulted in a brown-colored solution exhibiting a broad absorption peak at 422 nm. The color, defining the NSP5 preparation, gradually diminished upon exposure to ambient air, implying the presence of an oxygen-sensitive cofactor [71]. Inductively Coupled Plasma Optical Emission Spectroscopy (ICP-OES) indi-

cated the presence of iron, although at a lower-than-expected stoichiometry, suggesting that the protein solution obtained during aerobic purification consisted of a combination of apo- and holo-protein [71]. This outcome aligns with expectations for a FeS protein, given the well-known susceptibility of these cofactors to degradation when exposed to oxygen [18]. Further confirmation came from electron paramagnetic resonance (EPR) spectroscopy, which verified the existence of a [2Fe-2S] cluster coordinated by NSP5 and positioned at the interface between NSP5 dimers within the 169–179 region. Mutational analysis pinpointed two cysteine residues (Cys171 and Cys174) in NSP5 as ligands for the cluster [71]. The FeS-ligating residues demonstrated conservation across group A, C, and D rotaviruses, suggesting a shared capability among rotavirus NSP5 proteins to ligate a rhombic cluster.

Martin et al. showed that mutagenesis of the two cysteine residues responsible for FeS ligation did not hinder viroplasm formation [71]. However, the NSP5 protein devoid of the iron–sulfur cluster had different binding patterns to ssRNA [71]. The wild-type NSP5 exhibited two ssRNA-binding sites, as detected by microscale thermophoresis, whereas both the NSP5 with mutated cysteines (into alanines) and an "oxidized-NSP5" had only one ssRNA-binding site [71]. The FeS cluster in NSP5 appears to be involved in the binding of ssRNA and might help in orchestrating the complex replication of the eleven genomic segments [71]. Despite this discovery being reported in 2013, there has been limited subsequent exploration into the role of the FeS cluster in rotavirus NSP5 and the potential advantages it confers.

Additionally, to gain insights into the role of the cluster in the rotavirus NSP5 and understand how its ligation influences protein conformation and dimerization, it would be important to solve the structure of NSP5 with its FeS cluster in the form that binds to RNA. This structural information would provide valuable details about the coordination of the cluster, its environment, the interaction of NSP5 with RNA in the presence of the FeS cofactor, and the resultant impact on the conformation and dimeric/oligomeric state of the protein. Further investigation into the utilization of FeS clusters in rotavirus replication could expand our understanding of the mechanisms underlying rotavirus replication.

3.2. The Merkel Cell Polyomavirus Small T Antigen (sT)

The discovery of the Merkel cell polyomavirus small T antigen as a FeS protein was a fortuitous finding as well, highlighted by the brown color of the purified protein indicative of the presence of iron [77]. Merkel cell polyomavirus (MCPyV) is a small, circular double-stranded DNA (dsDNA) virus belonging to the *Polyomaviridae* family (Figure 3A) [78,79]. The MCPyV viral genome can clonally integrate into the host genome which is a significant event in the development of Merkel cell carcinoma (MCC), a rare but aggressive skin cancer [80,81]. Upon infection, MCPyV relies heavily on the host cell DNA replication machinery within the cell nucleus [79]. The viral DNA is released directly into the host cell's nucleus, following entry [79]. Subsequently, the cellular apparatus initiates the transcription of early genes from the MCPyV genome [79]. Among the early genes are the regulatory proteins large T antigen (LT) and small T antigen (sT) that play a crucial role in genome replication and MCPyV-related carcinogenesis [78].

Both LT and sT have an HSP40 chaperone J-like domain at their N terminus (Figure 3B) [78,82]. LT has a large helicase domain and a DNA origin binding domain (OBD) [78]. LT initiates genome replication by binding to seven sequence-specific sites along 71 bp of the circular genome, allowing the cellular replication enzymes to reach the DNA template and initiate replication (Figure 3C,D) [79]. sT was initially thought to enhance replication solely by increasing LT stability through the inhibition of the E3 ubiquitin ligase FBXW7 [77,83]. sT, a 22 kDa protein with a T-antigen-like domain on its C-terminal half (Figure 3E), was found to ligate two FeS clusters, a [2Fe-2S] and [4Fe-4S], within two metal binding pockets composed of cysteine residues, as assessed by EPR spectroscopy [77]. Tsang et al. showed that mutating the FeS-ligating residues of sT rendered the protein ineffective in stimulating LT-mediated viral DNA replication, highlighting the essential roles of these residues for sT function [77]. Moreover, these studies proposed

that sT can stabilize LT without altering its protein levels. sT was shown to localize to active replication sites at the viral origin where LT is known to act, indicating a more direct role of sT in viral genome replication [77]. A recent paper showed by knockout studies that while sT was not essential for initiating viral DNA replication, it played a crucial role in maintaining genome integrity and activating the transcription of early and late genes, specifically LT and VP1—the primary capsid protein [82]. Investigating the role of the FeS clusters for sT function could significantly advance our understanding of the function of sT in carcinogenesis.
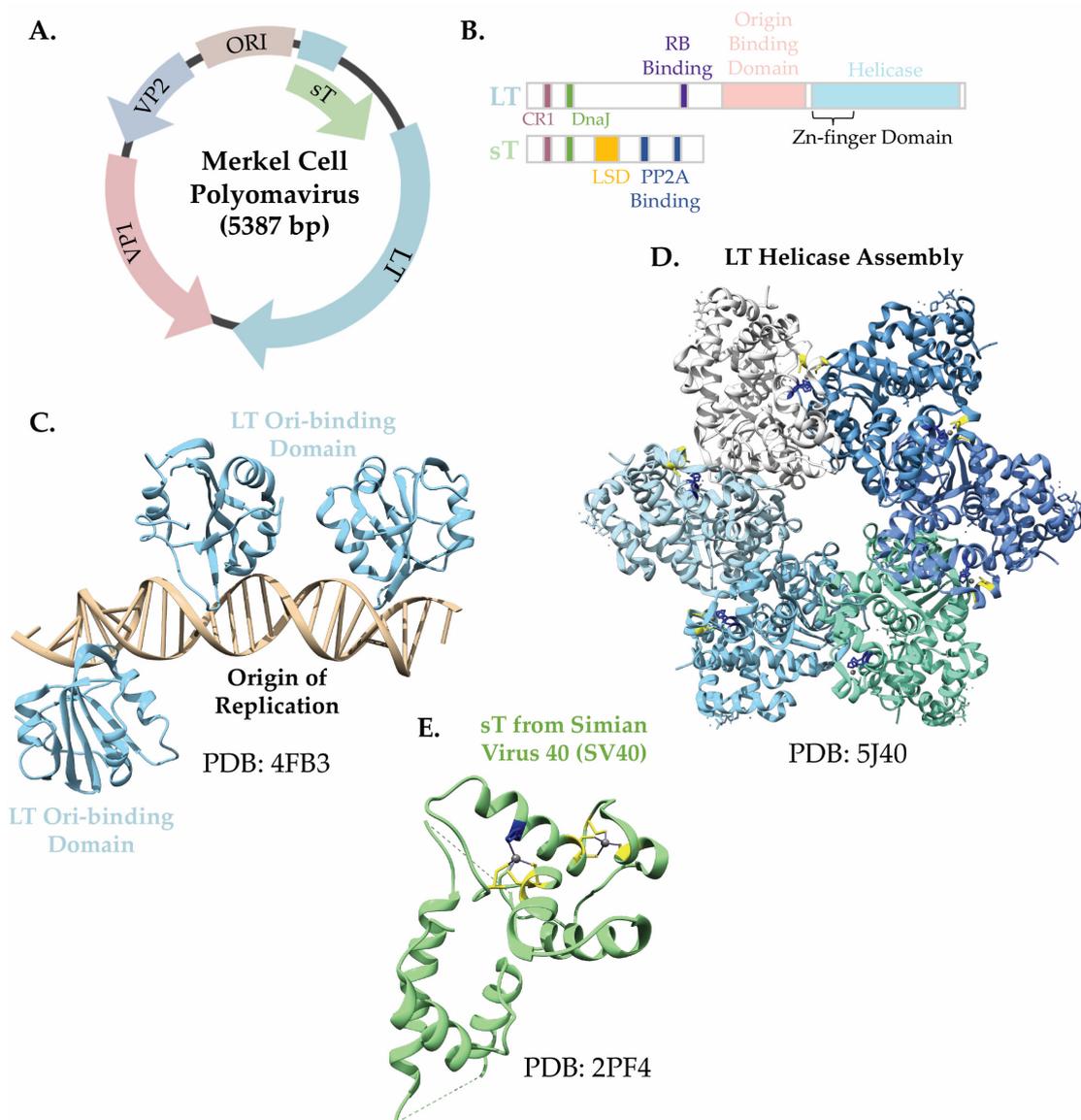

Figure 3. Merkel-cell polyomavirus, sT. (A) The circular double-stranded DNA (dsDNA) genome of Merkel cell polyomavirus undergoes replication within the cell nucleus through the involvement of cellular replication proteins [78]. **(B)** The early genes large T antigen (LT) and small-T antigen (sT) share N-terminal regions. LT comprises a C-terminal origin binding domain (OBD) and a helicase domain, while sT contains an LT stabilizing domain (LSD) and protein phosphatase 2A (PP2A) binding domains [78]. **(C)** Structure of LT OBD in complex with dsDNA at the replication origin (PDB: 4FB3). **(D)** The LT-helicase domain assembles as a heptamer. Zinc-ligating residues are highlighted (PDB: 5J40). **(E)** The structure of sT from a closely related virus SV40 exhibits similar metal-binding sites as sT of Merkel cell polyomavirus, which are highlighted (PDB: 2PF4). The figure was created with the assistance of BioRender.com.

3.3. The SARS-CoV-2 nsp12 and nsp13

The virus responsible for the COVID-19 pandemic, Severe Acute Respiratory Syndrome Coronavirus 2 (SARS-CoV-2), has been found to encode two FeS proteins that are at the core of the replication and transcription complex (RTC) (Figure 4A,B) [84,85]. This discovery came into focus amid the pandemic's heightened interest. The presence of LYR-like motifs and metal-binding sites in the viral proteins enabled the prediction of FeS-cluster-binding sites, subsequently experimentally confirmed, a finding that suggests the existence of FeS proteins hiding in plain sight.
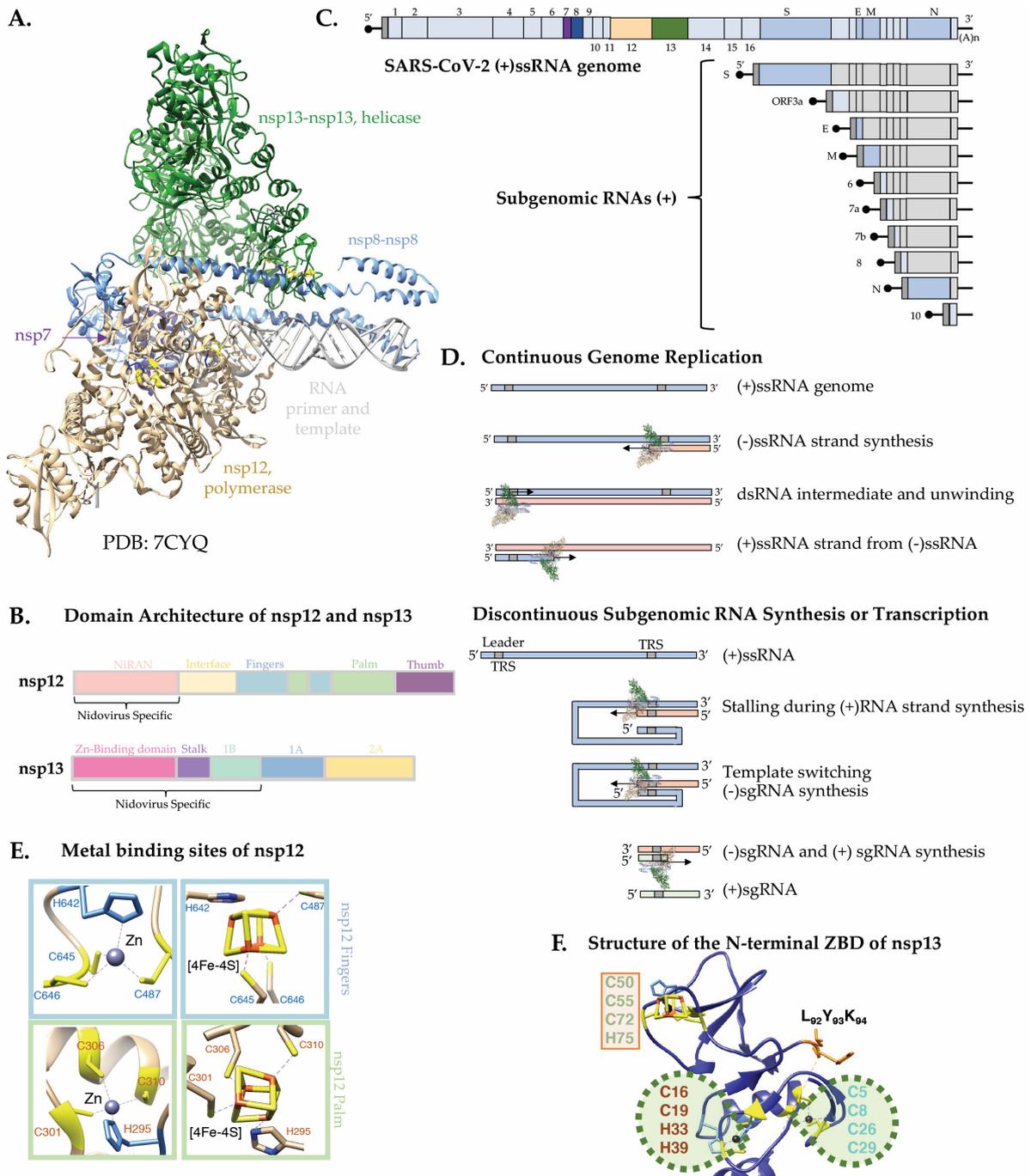

Figure 4. SARS-CoV-2 genome replication modes and structures of the RNA-dependent RNA polymerase, nsp12, and helicase, nsp13. (A) Structure of the SARS-CoV-2 RNA-dependent RNA polymerase (RdRp) consisting of nsp12, a dimer of nsp8 and nsp7, along with a dimer of the helicase

nsp13 and double-stranded primer-template RNA (PDB: 7CYQ). (**B**) Domain organization of nsp12 and nsp13 with nidovirus specific domains highlighted [86–89]. (**C**) Organization of the (+)ss-RNA genome of SARS-CoV-2 and (+) subgenomic RNAs that encode structural and accessory proteins [89,90]. (**D**) Schematic representation of continuous and discontinuous modes of SARS-CoV-2 replication. The continuous synthesis involves the replication of the (+)ssRNA genome into (-)ssRNA, forming double-stranded RNA as the product, with nsp13 unwinding the double-stranded RNA in the 5′–3′ direction. The (+)ssRNA strand is then synthesized using the (-)ssRNA as a template. On the other hand, discontinuous synthesis occurs at the 3′ end of the genome, where stalling during replication leads to template switching, allowing the 5′ leader sequence to serve as a template for the remaining (-) subgenomic RNA through base-pairing with the internal Transcription Regulatory Sequences (TRSs). This process results in the synthesis of the (+) subgenomic RNA using the (-) subgenomic RNA as a template [90,91]. The arrows indicate the directionality of replication. (**E**) Metal-binding sites within the catalytic domain of the SARS-CoV-2 RdRp and at the interface between the NiRAN and the catalytic domain. The coordination details of the zinc-binding residues are depicted in stick representation. The sites where FeS clusters have been experimentally confirmed to be ligated [84] are represented by modeling them in place of zinc, with their coordinate details shown in stick representation. (**F**) Depiction of the structure of the N-terminal Zinc Binding Domain (ZBD) of nsp13, illustrating the amino acid residues involved in zinc coordination, as observed in the available crystal structure (PDB ID: 6ZSL) [92].

SARS-CoV-2 is a coronavirus of the order *Nidovirales* [91,93,94]. Nidovirus genomes are known for their remarkable length, typically encompassing ~30,000 bases of single-stranded RNA (Figure 4C) [91,93,94]. The genomes of most RNA viruses are comparatively shorter, consisting of approximately 9000 bases [95], a difference that can be attributed to factors such as the use of low-fidelity polymerases and the inherent instability of RNA [89,94,96]. Coronaviruses stand out by encoding an exoribonuclease, an uncommon feature among RNA viruses, to counteract mutations as they arise during replication [91,94,96,97]. Upon entering a host cell and releasing its genome into the cytosol, coronaviruses utilize host ribosomes to translate two polypeptides directly from the positive sense-single-stranded RNA genome from two juxtaposed open reading frames defined through a ribosome frameshifting site [94,98]. The single polypeptides are cleaved by two viral proteases, namely nsp3 and nsp5, into sixteen non-structural proteins (nsps) [89,94,99]. A significant number of nsps assemble into the multisubunit RTC, responsible for replicating the RNA genome and transcribing structural and accessory genes [94]. The viral genome includes transcriptional regulatory sequences (TRS) located between the structural and accessory genes that are complementary to a 5′ leader sequence, enabling a template switching mechanism that skips large portions of the genome during transcription (Figure 4D) [89,91,94]. This complex mechanism ensures that each transcription product or subgenomic RNA (sgRNA) acquires a polyA tail and a 5′cap allowing for evasion of host defenses [86,89,91,94,100]. Moreover, this mechanism potentially accommodates the diverse copy number needs for structural and accessory proteins [94,100].

The heart of the replication and transcription complex of SARS-CoV-2 is nsp12, the catalytic subunit of the RNA-dependent RNA polymerase (RdRp), which adopts a right-hand conformation characterized by a unique N-terminal nidovirus-specific nucleotidyl transferase (NiRAN) domain [86]. Nsp12 was found to ligate two $[4Fe-4S]^{2+}$ clusters [84] in the same sites that had been modeled as zinc centers in the cryo-EM structures of the aerobically purified complex (Figure 4E) [101]. One FeS cluster is at the interface between the NiRAN and the catalytic domain and the second in the fingers subdomain within the polymerase domain (Figure 4B,E) [84]. Using an in vitro primer extension assay with the minimal requirements of nsp12 and the two accessory factors, nsp7 and nsp8, Maio and colleagues showed that the iron–sulfur cluster in the catalytic domain is essential for replication [84]. Substitution of the FeS-ligating residues in the polymerase domain abolished the activity of the RdRp [84]. The aerobically purified form of nsp12 containing zinc had significantly reduced polymerization efficiency and reduced affinity of binding to

the RNA template [84]. The template tested in this experiment was 1000 times smaller than the SARS-CoV-2 RNA genome and had minimal secondary structure [84]. Under these conditions, Zn was shown to be partially able to support function by potentially serving a structural role that preserved the integrity and tridimensional structure of the catalytic domain [84].

Mutagenesis of the FeS-ligating residues in the interface domain of nsp12 diminished its interaction with the SARS-CoV-2 helicase nsp13 without profoundly impairing the RNA polymerase activity [84]. Nsp13 is a member of the 1B superfamily of helicases (SF1B) with an ATP-dependent unwinding activity that proceeds in the 5′ to 3′ direction [102]. Notably, the directionality of nsp13 opposes that of nsp12, which extends the nascent RNA template in the 3′ to 5′ direction. Available cryo-EM structures of the SARS-CoV-2 RTC show two nsp13 protomers per copy of the RdRp (Figure 4A) [87,88]. While the significance of this arrangement is still under debate, it has been proposed that one of the two nsp13 protomers may allow backtracking of the RdRp and template switching, while the other would enable the unwinding of downstream RNA secondary structures [88]. Nsp13 is organized into five distinctive domains: an N-terminal Zinc Binding Domain (ZBD), a 1B beta barrel domain, a helical stalk and two RecA-like domains 1A and 2A, required for binding and hydrolysis of ATP (Figure 4B) [102,103]. Interestingly, nsp13 was also found to ligate a $[4Fe-4S]^{2+}$ cluster and two Zn^{2+} ions within its ZBD (Figure 4F) [85]. Aerobically purified nsp13 ligates three zinc ions in its ZBD and has been shown to exhibit a significantly higher activity on DNA in in vitro enzymatic assays, despite its physiological substrate being RNA [104–106]. To investigate the effect of the FeS cluster on nsp13 binding to RNA versus DNA, Maio and colleagues performed electrophoretic mobility shift assays (EMSAs) using either anoxically purified nsp13 ligating a FeS in its ZBD (Zn_2-[4Fe-4S]) or nsp13 purified aerobically and fully reconstituted with zinc (Zn_3) [85]. Nsp13-Zn_2-[4Fe-4S] had approximately 100-fold greater affinity for RNA than nsp13-Zn_3 [85]. Additionally, nsp13-Zn_3 exhibited higher affinity of binding for DNA than for RNA which is in agreement with results previously published for the aerobically purified enzyme [106]. These findings demonstrate that the [4Fe-4S] cluster significantly enhances the binding selectivity of nsp13 for its physiological substrate, RNA. In line with the increased affinity of nsp13-Zn_2-[4Fe-4S] for RNA when compared to nsp13-Zn_3, functional assays demonstrated that the helicase anoxically purified with the cluster exhibited superior unwinding activity compared to the aerobically purified enzyme containing three zinc ions per protomer [85]. Loss of the FeS cluster negatively affected the unwinding activity of the helicase, presumably due to a reduced binding of the variant to the substrate.

The coexistence of a diverse metal composition, encompassing both zinc and a [4Fe-4S] cluster in nsp13, has been reported only once previously, in the cleavage and polyadenylation specificity factor 30 [107]. Nsp13 acquires its [4Fe-4S] cluster through the interaction of its LYK motif with the FeS biogenesis machinery, as revealed in recent studies [85]. The mechanism governing zinc delivery to the protein is likely dependent on ZNG1, known for recognizing a unique Cys_6His_2 zinc finger domain in zinc-dependent metalloproteins. ZNG1 functions as a GTPase metallochaperone, directing Zn allocation to specific recipient proteins [108]. The ZBD of nsp13 features a Cys_6His_2 domain organized into a RING-like module, ligating two zinc ions [85]. The presence of the LYK motif and the Cys_6His_2 zinc finger domain in nsp13 across all seven human coronaviruses suggests that similar pathways may be employed by other coronaviruses to incorporate two zinc ions and a [4Fe-4S] cluster into their ZBDs.

While the evolutionary conservation of FeS-ligating centers in the SARS-CoV-2 proteins underscores their importance in potentially providing advantages that enhance viral fitness, the known vulnerability of FeS cofactors to oxidative damage presents an exploitable property for targeting infections. This strategic approach has been employed in coronavirus replication, both in cell culture models and in vivo using the Golden Syrian hamster model of COVID-19 [84,109].

A stable nitroxide small molecule, TEMPOL (4-hydroxy-2,2,6,6-tetramethylpiperidin-1-oxyl), has demonstrated effectiveness in two different animal models of human disorders [110,111]. TEMPOL oxidizes and disassembles the FeS cluster of cytosolic aconitase (IRP1), converting it into the apo-form that regulates cellular iron homeostasis [110,111]. In in vitro testing on the SARS-CoV-2 RdRp and helicase, TEMPOL induced the oxidative degradation of the FeS clusters in both enzymes, impairing their activities [84,85]. Treatment of SARS-CoV-2-infected cells with TEMPOL robustly inhibited viral replication at concentrations exceeding 0.2 mM [84]. Notably, TEMPOL treatment did not induce cytotoxicity at doses up to 5 mM, likely due to its limited access to the mitochondrial matrix where many FeS proteins are localized. Furthermore, TEMPOL exhibited reduced reactivity towards most host FeS proteins, characterized by a redox potential exceeding -600 mV. The increased reactivity of TEMPOL towards the FeS clusters in the SARS-CoV-2 RdRp and helicase is attributed to the unusually negative reduction potentials of these clusters (lower than -600 mV) [84], making them susceptible to oxidation and transition to the inherently unstable $[4Fe-4S]^{3+}$ state, which quickly degrades [18]. This process results in the inactivation of the core components of the SARS-CoV-2 RTC that rely on FeS clusters for their activity. Subsequent in vivo studies demonstrated the efficacy of TEMPOL in inhibiting viral replication in the Golden Syrian hamster model of COVID-19 [109]. The inhibitory effect was observed when the drug was administered 2 h before infection, leading to a significant decrease in viral lung loads and pathology, without affecting shedding from the upper respiratory tract [109]. These studies lay the foundation for further exploration of drugs with a similar mode of action as TEMPOL as potential SARS-CoV-2 therapies during active viral infection.

3.4. The Hepatitis B HBx Protein

Hepatitis B virus (HBV) poses a global health burden and contributes to liver-related disease and mortality [112]. The World Health Organization estimates that one third of HBV infected patients develop no symptoms, another third non-icteric hepatitis, and the remaining third jaundice-related hepatitis with nausea, fatigue, and hepatomegaly [112,113]. Fulminant hepatitis develops in less than one percent of HBV-infected individuals which can lead to severe liver damage and death [112]. In addition to acute hepatitis, there are also chronic cases which are predominant if HBV infection occurred at a young age [112]. In chronic HBV infection, pathogenesis typically starts with liver inflammation, followed by fibrosis, cirrhosis and ultimately formation of hepatocellular carcinoma [112–114].

HBV is an enveloped virus with a partially circular dsDNA genome of 3.2 kb that primarily infects primates with a specific tropism for hepatocytes [113,115]. Upon infection, the viral DNA enters the cell nucleus [116] where it is converted into an episomal circular DNA molecule by cellular DNA repair mechanisms [113,117,118]. The closed circular DNA serves as a template for transcription of the pre-genomic RNA, which is the precursor of the viral genomic dsDNA, and of four subgenomic viral RNAs which are translocated to the cytosol where they are translated [117]. Capsid core structures consist of the pre-genomic RNA, the viral polymerase (P), and the HBV core capsid protein, (HBcAg) [117]. In these formations, the P enzyme carries out reverse transcription of pre-genomic RNA, converting it into a partially circular dsDNA genome [117]. Normally, the reverse transcription process takes place inside capsids that envelop at the endoplasmic reticulum [113,117,119]. Nevertheless, reverse transcription can also happen within capsid structures located in intracellular regions that are shuttled to the nucleus [113,117].

HBx, also known as the HBV X protein, plays several crucial roles in inducing changes within the cell, ultimately leading to hepatocellular pathogenesis and the development of hepatocellular carcinoma [113]. While the complete structure of HBx remains elusive, an in silico 3D-modeling study (Figure 5A) revealed significant structural similarity between HBx and a DNA glycosylase [120]. The 16.5 kDa X protein consists of an N-terminal transactivator domain involved in signal transduction and a C-terminal domain required for nuclear transcriptional activation of both virally encoded and host genes (Figure 5B) [113].

Within the C-terminal domain there are several mitochondrial localization sequences (Figure 5B) [113]. Moreover, different isoforms of HBx arise from two in-frame translation initiation codons, resulting in distinct N-termini [113]. These isoforms may have differential localization and function within the cell. Nuclear HBx primarily activates transcription of viral encoded proteins, whereas cytoplasmic HBx targets signaling cascades and mitochondria [113]. In mitochondria, studies have linked HBx to generation of reactive oxygen species (ROS) and a decrease in mitochondrial membrane potential [113]. The generation of ROS is suggested to inhibit PTEN, a tumor suppressor, and is implicated in overall hepatocarcinogenesis [113].
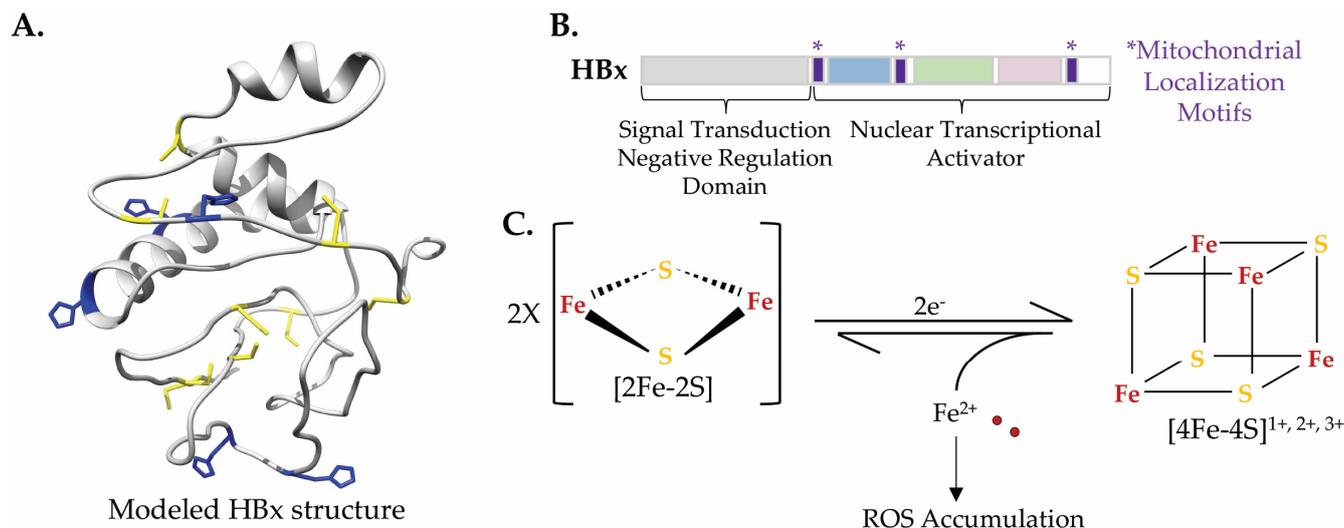

Figure 5. Hepatitis B Virus, HBx. (**A**) Computational model of HBx from van Hemert and colleagues, highlighting conserved histidines and cysteines marked in blue and yellow, respectively [120]. (**B**) Depiction of HBx domain architecture indicating the role of the N terminus in signal transduction and of the C terminus as a nuclear transcriptional activator [113]. (**C**) Diagram of cluster interconversion observed in HBx, as monitored by Mossbauer spectroscopy [121].

HBx has been associated with alterations in cellular iron homeostasis elicited by viral infection [122]. When expressed in Huh7 cells, HBx led to a reduction in both protein and mRNA levels of transferrin receptor 1 (TFR1) while increasing the protein and mRNA levels of ferritin [122]. Both TFR1 and ferritin mRNA levels are under the control of the iron regulatory proteins (IRP1 and IRP2) that bind specific RNA secondary structures called iron-responsive elements (IRE) [123–125]. Notably, upon HBx expression in Huh7 cells, a significant decrease in the protein levels of IRP1 was observed, leading to the proposal that HBx may influence cellular iron homeostasis by affecting IRP1 levels [122].

The biochemical and structural characterization of HBx has posed challenges, yet recent advancements have shed light on its properties. Notably, it has been discovered that HBx binds to a FeS cluster [121]. When solubility-tagged full-length HBx was purified, it was found to bind either a [2Fe-2S] or a [4Fe-4S] cluster, as confirmed by Mössbauer spectroscopy following growth in ^{57}Fe-enriched media [121]. The HBx-[2Fe-2S] was found to be stable upon exposure to atmospheric oxygen and could be converted to HBx-[4Fe-4S] upon addition of a strong reducing agent [121]. This interconversion was found to be partially reversible, allowing HBx-[4Fe-4S] to revert to HBx-[2Fe-2S] when exposed to oxygen (Figure 5C), albeit with some cluster degradation resulting in the release of mononuclear Fe^{3+} [121]. The FeS cluster in HBx appears to persist even after multiple rounds of oxidation and reduction, despite the accumulation of iron released upon cluster degradation (Figure 5C) [121]. The release of mononuclear iron is likely acting as a source of ROS potentially outside mitochondria or even in the nucleus [121]. The build-up of ROS

resulting from iron release during HBx-cluster redox events may contribute to the severity of liver disease and the development of carcinogenesis [121].

The reduction potential of the transition of the [4Fe-4S] cluster from the oxidized 2+ to the reduced 1+ state in HBx was determined to be ~-520 mV [121], close to the value measured for IscU (~-570 mV) [46]. This observation raises questions about the physiological relevance of this transition, given the necessity for a potent reductant to achieve cluster reduction. However, the binding of a partner protein or a small molecule could potentially enhance the reduction potential of the cluster.

A small amount of [2Fe-2S] cluster was detected in intact *E. coli* cells. The occurrence of the [2Fe-2S] cluster appeared to result from oxidative processes that converted the [4Fe-4S] cluster into a rhombic [2Fe-2S], yet its persistence in whole cells suggests a suboptimal ability of the *E. coli* biosynthetic apparatus to incorporate FeS clusters in precise stoichiometric amounts, particularly under conditions when proteins are overexpressed. This compromised insertion of FeS clusters might be mitigated by overexpressing HBx in mammalian or insect cells. Nonetheless, challenges persist due to the low solubility of HBx when isolated from insect cells and the variable overexpression of HBx in diverse mammalian cell lines, hampering these investigations, which remain crucial and should be pursued in the future.

The ability of HBx to coordinate both [2Fe-2S] and [4Fe-4S] clusters emerges as a common feature among sequences from the five examined HBV genotypes (A2, B, C, D, F1) [121]. With seven strictly conserved cysteines in its structure, HBx likely utilizes these residues as ligands of the cluster. Several of these conserved cysteine residues, such as C61, C69, and C137, play essential roles in HBx transactivation function [121]. Single-point substitutions of cysteine to alanine preserved FeS cluster incorporation, with complete loss occurring only in a variant lacking all cysteines [121]. These results indicate that, while cysteines are crucial for cofactor binding, HBx may adapt by utilizing alternative available cysteines to accommodate the FeS cluster. Among the conserved residues in HBx, cysteine residues 61, 69, and 137, and histidine 139 form a CCCH motif previously reported to coordinate Zn [126]. Interestingly, the expression of soluble HBx in a Zn-rich culture media competed with FeS cluster insertion [121], suggesting potential competitive ligation between these cofactors that share the same binding site. Historically, misclassification of many FeS cluster proteins as Zn proteins has occurred due to similar ligand requirements of the cofactors [127]. However, it is likely that in vivo, proper cofactor allocation is strictly regulated to prevent incorrect metal incorporation into a specific protein, which would potentially compromise its function.

The intriguing conversion of the FeS cluster in HBx from [2Fe-2S] to [4Fe-4S] under reducing conditions is reminiscent of conversions observed in FeS scaffold proteins [46,128]. However, the reductive coupling for HBx requires a strong reducing agent [121]. compared to A-type scaffolds and glutaredoxins. The precise physiological reductant for HBx remains unknown.

In summary, the HBV HBx protein has been found to coordinate either a $[2Fe-2S]^{2+}$ or a $[4Fe-4S]^{2+}$ as likely cofactors. The identification of an FeS cluster in HBx adds to the growing list of viral proteins characterized as FeS proteins and may provide new perspectives to uncover mechanisms underlying carcinogenesis in chronic HBV infection.

3.5. The Mimivirus GciS Protein

Mimiviruses are among the largest viruses found to date at roughly 750 nm in diameter with a linear dsDNA genome of approximately 12,000 kb [70]. Their denotation originates from "Mimicking Microbes", which was coined due to their ability to mimic bacteria in both size and appearance [70]. Mimiviruses are nucleocytoplasmic large DNA viruses (NCLDV), which also include *Poxviridae* and *Asfarviridae*, known to infect mammals [70,129]. Mimiviruses, however, infect *Acanthamoeba*, a unicellular amoeba [70]. Their genomes consist of an impressive 1262 open reading frames that encode unusual proteins, including tRNA synthetases, translation peptide release factors, 6 tRNAs, DNA repair glycosylases,

a UV-damage endonuclease, and type I and type II topoisomerases [70]. It is likely not a coincidence that many of these pathways rely on FeS clusters within cells.

GciS is a mimivirus glycine and cysteine-rich protein of approximately 6 kDa that was recently found to ligate FeS clusters of both the $[2Fe-2S]^{2+}$ and the linear $[3Fe-4S]^{1+}$ geometry as assessed by Mossbauer spectroscopy on the Fe^{57}-enriched purified protein (Figure 6A,B) [130]. The linear $[3Fe-4S]^{1+}$ cluster represents a rare arrangement in biological systems [131]. It may be an aerobically stabilized geometry in which loss of one Fe^{3+} atom would yield a [2Fe-2S] cluster or it may be a step in the process of formation of a [4Fe-4S] [131].

A.

MS**C**FGGWNGG**C**GP**C**GGFGWGG**C**GPSWG**C**GP**C**GFGGGYSY
RVSYGFPGGFGWGG**CC**

B.

$[2Fe-2S]^{2+}$
(Rhombic)
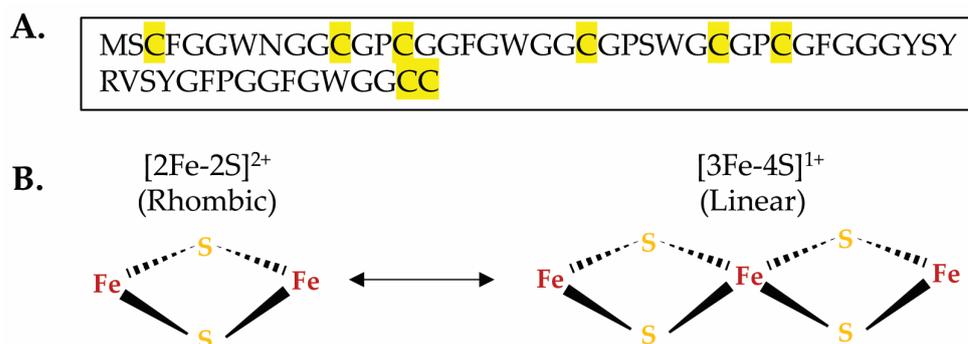
$[3Fe-4S]^{1+}$
(Linear)

Figure 6. Mimivirus, GciS. (**A**) Sequence of GciS with cysteines highlighted in yellow [130]. (**B**) Diagram of cluster interconversion observed in GciS by Mossbauer spectroscopy [130].

While GciS lacks a predicted structure, it has demonstrated the ability to oligomerize [130]. GciS was found to ligate 0.23 $[2Fe-2S]^{2+}$ clusters and 0.06 $[3Fe-4S]^{1+}$ clusters per monomer as estimated from Inductively Coupled Plasma Mass Spectrometry (ICP-MS) analysis, which corresponds to approximately 0.65 Fe atoms per monomer. This suggests that cysteines from multiple monomers are required to bind even a single [2Fe-2S] cluster [130]. In the case of glutaredoxins which have been shown to have similar FeS features, it is common for the FeS cluster to be bound by two cysteines from separate protein monomers along with two glutathione ligands [131]. Villalta and colleagues give a glance into a potentially widespread FeS proteome in Mimiviruses [130]. Further, they show that GciS-like proteins from clades A, B, C, and D of the *Megavirinae* family have UV–vis and EPR features suggestive of the presence of FeS clusters [130].

Future studies into the GciS proteins are warranted to gain insights into their physiological role. Such investigations may potentially uncover novel functions for viral FeS proteins.

4. Conclusions and Perspectives

4.1. Drawing Similarities

Table 1 outlines the five viruses that encode FeS proteins, all of which are discussed in this review. A prevailing theme emerges, indicating that many of these viral FeS proteins are involved in genome replication. Viruses have very diverse and complex genomic organizations, collectively encoding an assorted array of polymerases to replicate their genomes [132]. Viruses can be categorized in the Baltimore Classification according to their genome organization, as follows:

Group I: Double-stranded DNA viruses (MCPyV, Mimivirus);
Group II: Single-stranded DNA viruses;
Group III: Double-stranded RNA viruses (Rotavirus);
Group IV: Positive-sense single-stranded RNA viruses (SARS-CoV-2);
Group V: Negative-sense single-stranded RNA viruses;
Group VI: Single-stranded RNA viruses with a DNA intermediate;
Group VII: Double-stranded DNA viruses with an RNA intermediate (HBV).

Table 1. List of viruses thus far identified that encode FeS proteins.

Virus	Genome	Family	Host and Tropism	FeS Protein(s)	Stoichiometry and Oxidation States	Role of Protein(s)	Proposed Role of FeS Cluster	Reference	Date
Rotavirus	Segmented dsRNA	*Reoviridae*	Human, mature enterocytes of the villi of the small intestine	NSP5	[2Fe-2S]	Viral RNA Replication and Packaging, Viroplasm Formation	Either packaging and/or replication of viral genome by modulating RNA interaction	[71]	2013
Merkel Cell Polyomavirus	dsDNA	*Polyomaviridae*	Human, Merkel Cells	sT	[2Fe-2S], [4Fe-4S]	Promotes LT-mediated viral DNA replication by the host cell polymerases	FeS coordination is important for sT promotion of viral replication	[77]	2015
SARS-CoV-2	(+)ssRNA	*Coronaviridae*	Human, ACE2 and TMPRSS2 expressing cells	nsp12	$[4Fe-4S]^{2+}$, $[4Fe-4S]^{2+}$	Polymerase, Viral RNA replication and transcription	Allows coordination between replication proteins in the complex. Enhances processivity of polymerase.	[84]	2021
				nsp13	$[4Fe-4S]^{2+}$, Zn^{2+}, Zn^{2+}	dsRNA Helicase (5′ -> 3′)	Enhances binding specificity for RNA substrate and increases unwinding ability	[85]	2023
Hepatitis B	Partially dsDNA	*Hepadnaviridae*	Human, Hepatocytes	HbX	$[2Fe-2S]^{2+}$ -> $[4Fe-4S]^{2+}$	Viral replication, Plays role in carcinogenesis	Potential Scaffold-like protein for directing cellular FeS cluster production. Regulation of Fe homeostasis proteins. Cluster conversion leads to accumulation of ROS	[121]	2022
Mimivirus	dsDNA	*Mimivirinae*	Acanthamoeba, Eukaryotic Unicellular Organism	GciS	$[2Fe-2S]^{2+}$, $[3Fe-4S]^{1+}$	Unknown	Iron-sulfur Cluster Intermediate Scaffold	[130]	2023

Viruses must either encode genome replication proteins or manipulate cellular proteins not originally within their codebook to replicate their genomes. Incidentally, viruses encode some of the rarest polymerases and enzymes involved in nucleic acid processing. Further, within the same virus family, replication enzymes are the most well conserved and viral polymerases also serve as a means to categorize viruses in terms of evolutionary characteristics [133,134]. The presence of FeS clusters within viral polymerases or other highly conserved proteins offers valuable insights to understand viral evolution and the changes they undergo over time [133,134]. Questions arise about the depth of conservation of viral FeS proteins and when they first emerged. Notably, all the virally encoded FeS proteins discussed in this review originate from viruses infecting eukaryotes. GciS stands out as the sole virally encoded FeS protein found in a virus infecting a non-mammalian organism. While little has been reported on FeS cluster utilization by viruses infecting other branches of the tree of life, it is likely that they exist.

Merkel cell polyomavirus and hepatitis B viruses belong to distinct evolutionary families as evidenced by differences in their genome sequence homology: polyomavirus falls under *Polyomaviridae*, while hepatitis B virus is classified under *Hepadnaviridae*. However, they are related by the fact that they are non-retroviruses that are known to integrate into host genomes. HBV encodes a reverse transcriptase and integrates similarly to retroviruses [135]. Merkel cell polyomaviruses LT may be responsible for clonal integration into host genomes during cellular mitosis [81]. Additionally, virally encoded FeS proteins found in both viruses might contribute significantly to carcinogenesis. Both HBx and GciS demonstrate characteristics of FeS cluster scaffolds with the capability to enable cluster interconversion. Overall, these observations shed light on how viral proteins enable viruses to manipulate FeS cluster utilization by co-opting the cellular machinery responsible for their assembly.

4.2. So Why Do Viruses Utilize FeS Clusters?

FeS clusters offer benefits to viruses similar to those they provide to host cells, which possess intricate pathways for their assembly, for proper delivery to recipient proteins, and for repair of partially oxidized clusters. Given that virtually all cells depend on iron–sulfur clusters, it stands to reason that viruses infecting host cells would, either indirectly or as discussed in this review, directly rely on FeS clusters. However, it is worth noting that it is unclear whether all viruses encode FeS proteins. The question then arises: why have certain viruses evolved to directly utilize these cofactors while others might have not? Could the utilization of FeS clusters by viral proteins offer insights into the timing of their evolution and, consequently, the evolution of the viruses that encode them?

FeS clusters have been postulated to represent relics of early life on Earth, preceding a significant increase in atmospheric oxygen brought about by the emergence of photosynthetic organisms that took place approximately 2.1 to 2.4 billion years ago [136]. Following the "great oxygen event", there was likely a widespread extinction event followed by evolutionary adaptations aimed towards utilizing oxidized Fe^{3+} while devising mechanisms to prevent the reactivity of free iron in cells. This reactivity could lead to the generation of harmful reactive oxygen species via Fenton chemistry [2,18]. This occurrence creates a paradox regarding the perceived benefits of FeS clusters in DNA replication proteins, as their presence could potentially heighten the risk of DNA damage due to reactive oxygen species. Despite this, numerous DNA and RNA binding proteins in bacteria, archaea, eukaryotes, and now viruses rely on FeS clusters, indicating an indispensable function of this cofactor for genome replication and maintenance [6–9]. Viruses are important contributors to ecological gene pools, not only by integrating directly into host genomes and sometimes acquiring host genes, but also by influencing the natural selection of host genes that offer an immune advantage against viruses. Consequently, viruses adapt to counteract these evolving immune strategies.

It is conceivable that viral proteins utilizing FeS clusters are remnants of ancient polymerases, ssRNA binding proteins, and helicases that employed FeS clusters in an era

predating the "great oxygen event". These proteins have persisted throughout evolution due to the advantages they confer through natural selection.

The role of FeS clusters in viral proteins remains largely uncharacterized. In the case of SARS-CoV-2 nsp12 and nsp13, FeS cofactors were discovered to significantly enhance the affinity of binding to the physiological substrate RNA, thereby facilitating replication processivity and unwinding activities, respectively. Both nsp12 and nsp13 were initially mischaracterized as zinc proteins. Additional putative zinc-ligating proteins assemble into the RTC of SARS-CoV-2, including the exoribonuclease, nsp14, and the small nsp10 required for the activity of both nsp14 and the methyltransferase nsp16. This situation raises the possibility of multiple components within the replication and transcription machinery of SARS-CoV-2 potentially emerging as FeS proteins.

So, why does the viral replication machinery require numerous FeS cofactors? A plausible explanation lies in the very high energetic cost of building a virus and the inability of viruses to produce the energy required for their replication [137,138]. We postulate that FeS clusters in viral proteins may help the utilization of the stored reducing equivalents of the host cell to provide energy for viral replication. This mechanism is likely analogous to the coupling of electron transfer to proton pumping across the inner mitochondrial membrane observed in mitochondrial respiratory complex I, ultimately contributing to energy production [139].

We also direct the reader to Table 1 of this article, which lists viruses identified thus far that encode FeS proteins and provides a possible role for the cofactors in each instance.

4.3. A Note on Importance

Studying viral FeS proteins can offer valuable insights into mechanisms that are responsible for the fitness and adaptability of viruses. Additionally, exploring viral FeS proteins may broaden our knowledge about FeS clusters, their coordination geometries, redox chemistries, and more. For instance, biophysical studies on the mimivirus GciS protein have unveiled the presence in biological systems of the rare linear [3Fe-4S] geometries seldomly observed in vivo.

The identification of two FeS clusters in the SARS-CoV-2 RdRp highlighted the importance of FeS proteins in viral replication. This discovery is especially noteworthy because the RdRp, being a highly conserved protein in rapidly mutating coronaviruses, represents an ideal target for antiviral therapeutics, much needed during the global pandemic [109]. The use of a FeS cluster-targeting technology was pioneered as an antiviral therapeutic strategy against SARS-CoV-2 infections [84,109], marking a groundbreaking development likely to be followed by further advancements.

Presently, we stand at the cusp of an exponential discovery phase of novel FeS proteins. Many of the viral FeS proteins discussed in this review were stumbled upon accidentally. Now, armed with knowledge, we have a clearer understanding of where and how to search for candidate FeS proteins aided by the identification of evolutionarily conserved LYR-like motifs and potential metal-binding sites in the structures of the proteins, when available, that can provide FeS cluster ligation sites.

Conflicts of Interest: The authors declare no conflict of interest.

References

1. Beinert, H.; Holm, R.H.; Munck, E. Iron-Sulfur Clusters: Nature's Modular, Multipurpose Structures. *Science* **1997**, *277*, 653–659. [CrossRef]
2. Sanchez, M.; Sabio, L.; Galvez, N.; Capdevila, M.; Dominguez-Vera, J.M. Iron chemistry at the service of life. *IUBMB Life* **2017**, *69*, 382–388. [CrossRef] [PubMed]
3. Letts, J.A.; Sazanov, L.A. Clarifying the supercomplex: The higher-order organization of the mitochondrial electron transport chain. *Nat. Struct. Mol. Biol.* **2017**, *24*, 800–808. [CrossRef]
4. Rouault, T.A.; Maio, N. Biogenesis and functions of mammalian iron-sulfur proteins in the regulation of iron homeostasis and pivotal metabolic pathways. *J. Biol. Chem.* **2017**, *292*, 12744–12753. [CrossRef] [PubMed]
5. Sickerman, N.S.; Ribbe, M.W.; Hu, Y. Nitrogenase Cofactor Assembly: An Elemental Inventory. *ACC Chem. Res.* **2017**, *50*, 2834–2841. [CrossRef]
6. Bartels, P.L.; Stodola, J.L.; Burgers, P.M.J.; Barton, J.K. A Redox Role for the [4Fe4S] Cluster of Yeast DNA Polymerase delta. *J. Am. Chem. Soc.* **2017**, *139*, 18339–18348. [CrossRef] [PubMed]
7. Barton, J.K.; Silva, R.M.B.; O'Brien, E. Redox Chemistry in the Genome: Emergence of the [4Fe4S] Cofactor in Repair and Replication. *Annu. Rev. Biochem.* **2019**, *88*, 163–190. [CrossRef]
8. O'Brien, E.; Holt, M.E.; Thompson, M.K.; Salay, L.E.; Ehlinger, A.C.; Chazin, W.J.; Barton, J.K. The [4Fe4S] cluster of human DNA primase functions as a redox switch using DNA charge transport. *Science* **2017**, *355*, eaag1789. [CrossRef]
9. Pinto, M.N.; Ter Beek, J.; Ekanger, L.A.; Johansson, E.; Barton, J.K. The [4Fe4S] Cluster of Yeast DNA Polymerase epsilon Is Redox Active and Can Undergo DNA-Mediated Signaling. *J. Am. Chem. Soc.* **2021**, *143*, 16147–16153. [CrossRef]
10. Barthelme, D.; Dinkelaker, S.; Albers, S.V.; Londei, P.; Ermler, U.; Tampe, R. Ribosome recycling depends on a mechanistic link between the FeS cluster domain and a conformational switch of the twin-ATPase ABCE1. *Proc. Natl. Acad. Sci. USA* **2011**, *108*, 3228–3233. [CrossRef]
11. Liu, G.; Sil, D.; Maio, N.; Tong, W.H.; Bollinger, J.M., Jr.; Krebs, C.; Rouault, T.A. Heme biosynthesis depends on previously unrecognized acquisition of iron-sulfur cofactors in human amino-levulinic acid dehydratase. *Nat. Commun.* **2020**, *11*, 6310. [CrossRef] [PubMed]
12. Dailey, H.A.; Finnegan, M.G.; Johnson, M.K. Human ferrochelatase is an iron-sulfur protein. *Biochemistry* **1994**, *33*, 403–407. [CrossRef] [PubMed]
13. Booker, S.J.; Lloyd, C.T. Twenty Years of Radical SAM! The Genesis of the Superfamily. *ACS Bio Med Chem Au* **2022**, *2*, 538–547. [CrossRef] [PubMed]
14. Wang, H.; Shi, H.; Rajan, M.; Canarie, E.R.; Hong, S.; Simoneschi, D.; Pagano, M.; Bush, M.F.; Stoll, S.; Leibold, E.A.; et al. FBXL5 Regulates IRP2 Stability in Iron Homeostasis via an Oxygen-Responsive [2Fe2S] Cluster. *Mol. Cell* **2020**, *78*, 31–41.e5. [CrossRef] [PubMed]
15. Rouault, T.A.; Maio, N. How Oxidation of a Unique Iron-Sulfur Cluster in FBXL5 Regulates IRP2 Levels and Promotes Regulation of Iron Metabolism Proteins. *Mol. Cell* **2020**, *78*, 1–3. [CrossRef] [PubMed]
16. Holm, R.H.; Lo, W. Structural Conversions of Synthetic and Protein-Bound Iron-Sulfur Clusters. *Chem. Rev.* **2016**, *116*, 13685–13713. [CrossRef] [PubMed]
17. Bromberg, Y.; Aptekmann, A.A.; Mahlich, Y.; Cook, L.; Senn, S.; Miller, M.; Nanda, V.; Ferreiro, D.; Falkowski, P. Quantifying structural relationships of metal-binding sites suggests origins of biological electron transfer. *Sci. Adv.* **2022**, *8*, eabj3984. [CrossRef] [PubMed]
18. Imlay, J.A. Iron-sulphur clusters and the problem with oxygen. *Mol. Microbiol.* **2006**, *59*, 1073–1082. [CrossRef]
19. McKeown, S.R. Defining normoxia, physoxia and hypoxia in tumours-implications for treatment response. *Br. J. Radiol.* **2014**, *87*, 20130676. [CrossRef]
20. Thomas, K.A. Angiogenesis. In *Encyclopedia of Cell Biology*; Academic Press: Cambridge, MA, USA, 2016; pp. 102–116, ISBN 9780123947963.
21. Pandelia, M.E.; Lanz, N.D.; Booker, S.J.; Krebs, C. Mossbauer spectroscopy of Fe/S proteins. *Biochim. Biophys. Acta* **2015**, *1853*, 1395–1405. [CrossRef]
22. Cutsail, G.E., 3rd; Telser, J.; Hoffman, B.M. Advanced paramagnetic resonance spectroscopies of iron-sulfur proteins: Electron nuclear double resonance (ENDOR) and electron spin echo envelope modulation (ESEEM). *Biochim. Biophys. Acta* **2015**, *1853*, 1370–1394. [CrossRef] [PubMed]
23. Crack, J.C.; Le Brun, N.E. Native Mass Spectrometry of Iron-Sulfur Proteins. In *Fe-S Proteins: Methods and Protocols*; Dos Santos, P.C., Ed.; Springer: New York, NY, USA, 2021; pp. 231–258. [CrossRef]
24. Maio, N.; Rouault, T.A. Outlining the Complex Pathway of Mammalian Fe-S Cluster Biogenesis. *Trends Biochem. Sci.* **2020**, *45*, 411–426. [CrossRef] [PubMed]
25. Genova, M.L.; Lenaz, G. Functional role of mitochondrial respiratory supercomplexes. *Biochim. Biophys. Acta* **2014**, *1837*, 427–443. [CrossRef] [PubMed]
26. Carroll, B.L.; Zahn, K.E.; Hanley, J.P.; Wallace, S.S.; Dragon, J.A.; Doublie, S. Caught in motion: Human NTHL1 undergoes interdomain rearrangement necessary for catalysis. *Nucleic Acids Res.* **2021**, *49*, 13165–13178. [CrossRef] [PubMed]

27. Maio, N.; Rouault, T.A. Mammalian iron sulfur cluster biogenesis: From assembly to delivery to recipient proteins with a focus on novel targets of the chaperone and co-chaperone proteins. *IUBMB Life* **2022**, *74*, 684–704. [CrossRef] [PubMed]

28. Ciesielski, S.J.; Schilke, B.A.; Osipiuk, J.; Bigelow, L.; Mulligan, R.; Majewska, J.; Joachimiak, A.; Marszalek, J.; Craig, E.A.; Dutkiewicz, R. Interaction of J-protein co-chaperone Jac1 with Fe-S scaffold Isu is indispensable in vivo and conserved in evolution. *J. Mol. Biol.* **2012**, *417*, 1–12. [CrossRef]

29. Chakrabbarti, M.; Lindahl, P.A. The utility of Mossbauer spectroscopy in eukaryotic cell biology and animal physiology. In *Iron-Sulfur Clusters in Chemistry and Biology*; Rouault, T.A., Ed.; Walter de Gruyter: Berlin, Germany; Boston, MA, USA, 2014; pp. 49–71.

30. Maio, N.; Rouault, T.A. Iron-sulfur cluster biogenesis in mammalian cells: New insights into the molecular mechanisms of cluster delivery. *Biochim. Biophys. Acta* **2015**, *1853*, 1493–1512. [CrossRef]

31. Li, K.; Tong, W.-H.; Hughes, R.M.; Rouault, T.A. Roles of the Mammalian Cytosolic Cysteine Desulfurase, ISCS, and Scaffold Protein, ISCU, in Iron-Sulfur Cluster Assembly. *J. Biol. Chem.* **2006**, *281*, 12344–12351. [CrossRef]

32. Tong, W.H.; Rouault, T.A. Distinct iron-sulfur cluster assembly complexes exist in the cytosol and mitochondria of human cells. *EMBO* **2000**, *19*, 5692–5700. [CrossRef]

33. Tong, W.H.; Rouault, T.A. Functions of mitochondrial ISCU and cytosolic ISCU in mammalian iron-sulfur cluster biogenesis and iron homeostasis. *Cell Metab.* **2006**, *3*, 199–210. [CrossRef]

34. Srour, B.; Gervason, S.; Hoock, M.H.; Monfort, B.; Want, K.; Larkem, D.; Trabelsi, N.; Landrot, G.; Zitolo, A.; Fonda, E.; et al. Iron Insertion at the Assembly Site of the ISCU Scaffold Protein Is a Conserved Process Initiating Fe-S Cluster Biosynthesis. *J. Am. Chem. Soc.* **2022**, *144*, 17496–17515. [CrossRef] [PubMed]

35. Shi, R.; Proteau, A.; Villarroya, M.; Moukadiri, I.; Zhang, L.; Trempe, J.F.; Matte, A.; Armengod, M.E.; Cygler, M. Structural basis for Fe-S cluster assembly and tRNA thiolation mediated by IscS protein-protein interactions. *PLoS Biol.* **2010**, *8*, e1000354. [CrossRef] [PubMed]

36. Adam, A.C.; Bornhovd, C.; Prokisch, H.; Neupert, W.; Hell, K. The Nfs1 interacting protein Isd11 has an essential role in Fe/S cluster biogenesis in mitochondria. *EMBO J.* **2006**, *25*, 174–183. [CrossRef] [PubMed]

37. Shi, Y.; Ghosh, M.C.; Tong, W.H.; Rouault, T.A. Human ISD11 is essential for both iron-sulfur cluster assembly and maintenance of normal cellular iron homeostasis. *Hum. Mol. Genet.* **2009**, *18*, 3014–3025. [CrossRef]

38. Terali, K.; Beavil, R.L.; Pickersgill, R.W.; van der Giezen, M. The effect of the adaptor protein Isd11 on the quaternary structure of the eukaryotic cysteine desulphurase Nfs1. *Biochem. Biophys. Res. Commun.* **2013**, *440*, 235–240. [CrossRef] [PubMed]

39. Patel, S.J.; Frey, A.G.; Palenchar, D.J.; Achar, S.; Bullough, K.Z.; Vashisht, A.; Wohlschlegel, J.A.; Philpott, C.C. A PCBP1-BolA2 chaperone complex delivers iron for cytosolic [2Fe-2S] cluster assembly. *Nat. Chem. Biol.* **2019**, *15*, 872–881. [CrossRef]

40. Shi, H.; Bencze, K.Z.; Stemmler, T.L.; Philpott, C.C. A cytosolic iron chaperone that delivers iron to ferritin. *Science* **2008**, *320*, 1207–1210.

41. Nandal, A.; Ruiz, J.C.; Subramanian, P.; Ghimire-Rijal, S.; Sinnamon, R.A.; Stemmler, T.L.; Bruick, R.K.; Philpott, C.C. Activation of the HIF prolyl hydroxylase by the iron chaperones PCBP1 and PCBP2. *Cell Metab.* **2011**, *14*, 647–657. [CrossRef]

42. Leidgens, S.; Bullough, K.Z.; Shi, H.; Li, F.; Shakoury-Elizeh, M.; Yabe, T.; Subramanian, P.; Hsu, E.; Natarajan, N.; Nandal, A.; et al. Each member of the poly-r(C)-binding protein 1 (PCBP) family exhibits iron chaperone activity toward ferritin. *J. Biol. Chem.* **2013**, *288*, 17791–17802. [CrossRef]

43. Frey, A.G.; Nandal, A.; Park, J.H.; Smith, P.M.; Yabe, T.; Ryu, M.S.; Ghosh, M.C.; Lee, J.; Rouault, T.A.; Park, M.H.; et al. Iron chaperones PCBP1 and PCBP2 mediate the metallation of the dinuclear iron enzyme deoxyhypusine hydroxylase. *Proc. Natl. Acad. Sci. USA* **2014**, *111*, 8031–8036. [CrossRef]

44. Boniecki, M.T.; Freibert, S.A.; Muhlenhoff, U.; Lill, R.; Cygler, M. Structure and functional dynamics of the mitochondrial Fe/S cluster synthesis complex. *Nat. Commun.* **2017**, *8*, 1287. [CrossRef] [PubMed]

45. Cai, K.; Tonelli, M.; Frederick, R.O.; Markley, J.L. Human Mitochondrial Ferredoxin 1 (FDX1) and Ferredoxin 2 (FDX2) Both Bind Cysteine Desulfurase and Donate Electrons for Iron-Sulfur Cluster Biosynthesis. *Biochemistry* **2017**, *56*, 487–499. [CrossRef] [PubMed]

46. Chandramouli, K.; Unciuleac, M.C.; Naik, S.; Dean, D.R.; Huynh, B.H.; Johnson, M.K. Formation and properties of [4Fe-4S] clusters on the IscU scaffold protein. *Biochemistry* **2007**, *46*, 6804–6811. [CrossRef] [PubMed]

47. Tse, E.C.M.; Zwang, T.J.; Barton, J.K. The Oxidation State of [4Fe4S] Clusters Modulates the DNA-Binding Affinity of DNA Repair Proteins. *J. Am. Chem. Soc.* **2017**, *139*, 12784–12792. [CrossRef] [PubMed]

48. Voisine, C.; Cheng, Y.C.; Ohlson, M.; Schilke, B.; Hoff, K.; Beinert, H.; Marszalek, J.; Craig, E.A. Jac1, a mitochondrial J-type chaperone, is involved in the biogenesis of Fe/S clusters in Saccharomyces cerevisiae. *Proc. Natl. Acad. Sci. USA* **2001**, *98*, 1483–1488. [CrossRef] [PubMed]

49. Cupp-Vickery, J.R.; Peterson, J.C.; Ta, D.T.; Vickery, L.E. Crystal structure of the molecular chaperone HscA substrate binding domain complexed with the IscU recognition peptide ELPPVKIHC. *J. Mol. Biol.* **2004**, *342*, 1265–1278. [CrossRef]

50. Maio, N.; Singh, A.; Uhrigshardt, H.; Saxena, N.; Tong, W.H.; Rouault, T.A. Cochaperone binding to LYR motifs confers specificity of iron sulfur cluster delivery. *Cell Metab.* **2014**, *19*, 445–457. [CrossRef]

51. Marszalek, J.; Craig, E.A. Interaction of client-the scaffold on which FeS clusters are build-with J-domain protein Hsc20 and its evolving Hsp70 partners. *Front. Mol. Biosci.* **2022**, *9*, 1034453. [CrossRef]

52. Maio, N.; Kim, K.S.; Singh, A.; Rouault, T.A. A Single Adaptable Cochaperone-Scaffold Complex Delivers Nascent Iron-Sulfur Clusters to Mammalian Respiratory Chain Complexes I–III. *Cell Metab.* **2017**, *25*, 945–953.e6. [CrossRef]

53. Kampinga, H.H.; Craig, E.A. The HSP70 chaperone machinery: J proteins as drivers of functional specificity. *Nat. Rev. Mol. Cell Biol.* **2010**, *11*, 579–592. [CrossRef]

54. Sahi, C.; Craig, E.A. Network of general and specialty J protein chaperones of the yeast cytosol. *Proc. Natl. Acad. Sci. USA* **2007**, *104*, 7163–7168. [CrossRef] [PubMed]

55. Bonomi, F.; Iametti, S.; Morleo, A.; Ta, D.; Vickery, L.E. Facilitated transfer of IscU-[2Fe2S] clusters by chaperone-mediated ligand exchange. *Biochemistry* **2011**, *50*, 9641–9650. [CrossRef] [PubMed]

56. Dutkiewicz, R.; Schilke, B.; Cheng, S.; Knieszner, H.; Craig, E.A.; Marszalek, J. Sequence-specific interaction between mitochondrial Fe-S scaffold protein Isu and Hsp70 Ssq1 is essential for their in vivo function. *J. Biol. Chem.* **2004**, *279*, 29167–29174. [CrossRef]

57. Hoff, K.G.; Cupp-Vickery, J.R.; Vickery, L.E. Contributions of the LPPVK motif of the iron-sulfur template protein IscU to interactions with the Hsc66-Hsc20 chaperone system. *J. Biol. Chem.* **2003**, *278*, 37582–37589. [CrossRef] [PubMed]

58. Rouault, T.A. Mammalian iron-sulphur proteins: Novel insights into biogenesis and function. *Nat. Rev. Mol. Cell Biol.* **2015**, *16*, 45–55. [CrossRef]

59. Gari, K.; Ortiz, A.M.L.; Borel, V.; Flynn, H.; Skehel, J.M.; Boulton, S.J. MMS19 links cytoplasmic iron-sulfur cluster assembly to DNA metabolism. *Science* **2012**, *337*, 243–245. [CrossRef] [PubMed]

60. Stehling, O.; Vashisht, A.A.; Mascarenhas, J.; Jonsson, Z.O.; Sharma, T.; Netz, D.J.; Pierik, A.J.; Wohlschlegel, J.A.; Lill, R. MMS19 assembles iron-sulfur proteins required for DNA metabolism and genomic integrity. *Science* **2012**, *337*, 195–199. [CrossRef]

61. Kim, K.S.; Maio, N.; Singh, A.; Rouault, T.A. Cytosolic HSC20 integrates de novo iron-sulfur cluster biogenesis with the CIAO1-mediated transfer to recipients. *Hum. Mol. Genet.* **2018**, *27*, 837–852. [CrossRef]

62. Lill, R.; Freibert, S.A. Mechanisms of Mitochondrial Iron-Sulfur Protein Biogenesis. *Annu. Rev. Biochem.* **2020**, *89*, 471–499. [CrossRef]

63. Kassube, S.A.; Thoma, N.H. Structural insights into Fe-S protein biogenesis by the CIA targeting complex. *Nat. Struct. Mol. Biol.* **2020**, *27*, 735–742. [CrossRef]

64. Ye, H.; Rouault, T.A. Human iron-sulfur cluster assembly, cellular iron homeostasis, and disease. *Biochemistry* **2010**, *49*, 4945–4956. [CrossRef] [PubMed]

65. Maio, N.; Orbach, R.; Zaharieva, I.; Töpf, A.; Donkervoort, S.; Munot, P.; Mueller, J.; Willis, T.; Verma, S.; Peric, S.; et al. Loss of Function of the Cytoplasmic Fe-S Assembly Protein CIAO1 Causes a Neuromuscular Disorder with Compromise of Nucleocytoplasmic Fe-S Enzymes. *medRxiv* **2023**. [CrossRef]

66. Crick, F.H.C.; Watson, J.D. Structure of Small Viruses. *Nature* **1956**, *177*, 473–475. [CrossRef] [PubMed]

67. Wolf, Y.I.; Kazlauskas, D.; Iranzo, J.; Lucia-Sanz, A.; Kuhn, J.H.; Krupovic, M.; Dolja, V.V.; Koonin, E.V. Origins and Evolution of the Global RNA Virome. *mBio* **2018**, *9*, e02329-18. [CrossRef]

68. Twarock, R.; Luque, A. Structural puzzles in virology solved with an overarching icosahedral design principle. *Nat. Commun.* **2019**, *10*, 4414. [CrossRef]

69. Colson, P.; De Lamballerie, X.; Yutin, N.; Asgari, S.; Bigot, Y.; Bideshi, D.K.; Cheng, X.W.; Federici, B.A.; Van Etten, J.L.; Koonin, E.V.; et al. "Megavirales", a proposed new order for eukaryotic nucleocytoplasmic large DNA viruses. *Arch. Virol.* **2013**, *158*, 2517–2521. [CrossRef]

70. Raoult, D.; Audic, S.; Robert, C.; Abergel, C.; Renesto, P.; Ogata, H.; Scola, B.; Suzan, M.; Claverie, J. The 1.2-Mb Genome Sequence of Mimivirus. *Science* **2004**, *306*, 1344–1350. [CrossRef]

71. Martin, D.; Charpilienne, A.; Parent, A.; Boussac, A.; D'Autreaux, B.; Poupon, J.; Poncet, D. The rotavirus nonstructural protein NSP5 coordinates a [2Fe-2S] iron-sulfur cluster that modulates interaction to RNA. *FASEB J.* **2013**, *27*, 1074–1083. [CrossRef]

72. Ozsari, T.; Bora, G.; Kaya, B.; Yakut, K. The Prevalence of Rotavirus and Adenovirus in the Childhood Gastroenteritis. *Jundishapur J. Microbiol.* **2016**, *9*, e34867. [CrossRef] [PubMed]

73. Papa, G.; Borodavka, A.; Desselberger, U. Viroplasms: Assembly and Functions of Rotavirus Replication Factories. *Viruses* **2021**, *13*, 1349. [CrossRef]

74. Martin, D.; Ouldali, M.; Menetrey, J.; Poncet, D. Structural organisation of the rotavirus nonstructural protein NSP5. *J. Mol. Biol.* **2011**, *413*, 209–221. [CrossRef] [PubMed]

75. Fabbretti, E.; Afrikanova, I.; Vascotto, F.; Burrone, O.R. Two non-structural rotavirus proteins, NSP2 and NSP5, form viroplasm-like structures in vivo. *J. Gen. Virol.* **1999**, *80*, 333–339. [CrossRef] [PubMed]

76. Papa, G.; Venditti, L.; Arnoldi, F.; Schraner, E.M.; Potgieter, C.; Borodavka, A.; Eichwald, C.; Burrone, O.R. Recombinant Rotaviruses Rescued by Reverse Genetics Reveal the Role of NSP5 Hyperphosphorylation in the Assembly of Viral Factories. *J. Virol.* **2019**, *94*, e01110-19. [CrossRef] [PubMed]

77. Tsang, S.H.; Wang, R.; Nakamaru-Ogiso, E.; Knight, S.A.; Buck, C.B.; You, J. The Oncogenic Small Tumor Antigen of Merkel Cell Polyomavirus Is an Iron-Sulfur Cluster Protein That Enhances Viral DNA Replication. *J. Virol.* **2016**, *90*, 1544–1556. [CrossRef]

78. Wendzicki, J.A.; Moore, P.S.; Chang, Y. Large T and small T antigens of Merkel cell polyomavirus. *Curr. Opin. Virol.* **2015**, *11*, 38–43. [CrossRef]

79. Kwun, H.J.; Guastafierro, A.; Shuda, M.; Meinke, G.; Bohm, A.; Moore, P.S.; Chang, Y. The minimum replication origin of merkel cell polyomavirus has a unique large T-antigen loading architecture and requires small T-antigen expression for optimal replication. *J. Virol.* **2009**, *83*, 12118–12128. [CrossRef] [PubMed]

80. Becker, J.C.; Stang, A.; DeCaprio, J.A.; Cerroni, L.; Lebbe, C.; Veness, M.; Nghiem, P. Merkel cell carcinoma. *Nat. Rev. Dis. Primers* **2017**, *3*, 17077. [CrossRef]

81. Feng, H.; Shuda, M.; Chang, Y.; Moore, P.S. Clonal Integration of a polyomavirus in human Merkel cell carcinoma. *Science* **2008**, *319*, 1096–1100. [CrossRef]

82. Rapchak, K.; Yagobian, S.D.; Moore, J.; Khattri, M.; Shuda, M. Merkel cell polyomavirus small T antigen is a viral transcription activator that is essential for viral genome maintenance. *PLoS Pathog.* **2022**, *18*, e1011039. [CrossRef]

83. Kwun, H.J.; Shuda, M.; Feng, H.; Camacho, C.J.; Moore, P.S.; Chang, Y. Merkel cell polyomavirus small T antigen controls viral replication and oncoprotein expression by targeting the cellular ubiquitin ligase SCFFbw7. *Cell Host Microbe* **2013**, *14*, 125–135. [CrossRef]

84. Maio, N.; Lafont, B.A.P.; Sil, D.; Li, Y.; Bollinger, J.M., Jr.; Krebs, C.; Pierson, T.C.; Linehan, W.M.; Rouault, T.A. Fe-S cofactors in the SARS-CoV-2 RNA-dependent RNA polymerase are potential antiviral targets. *Science* **2021**, *373*, 236–241. [CrossRef] [PubMed]

85. Maio, N.; Raza, M.K.; Li, Y.; Zhang, D.; Bollinger, J.M., Jr.; Krebs, C.; Rouault, T.A. An iron-sulfur cluster in zinc-binding domain of the SARS-CoV-2 helicase modulates its RNA binding and unwinding activities. *Proc. Natl. Acad. Sci. USA* **2023**, *120*, e2303860120. [CrossRef] [PubMed]

86. Hillen, H.S.; Kokic, G.; Farnung, L.; Dienemann, C.; Tegunov, D.; Cramer, P. Structure of replicating SARS-CoV-2 polymerase. *Nature* **2020**, *584*, 154–156. [CrossRef]

87. Yan, L.; Ge, J.; Zheng, L.; Zhang, Y.; Gao, Y.; Wang, T.; Huang, Y.; Yang, Y.; Gao, S.; Li, M.; et al. Cryo-EM Structure of an Extended SARS-CoV-2 Replication and Transcription Complex Reveals an Intermediate State in Cap Synthesis. *Cell* **2021**, *184*, 184–193.e10. [CrossRef] [PubMed]

88. Chen, J.; Wang, Q.; Malone, B.; Llewellyn, E.; Pechersky, Y.; Maruthi, K.; Eng, E.T.; Perry, J.K.; Campbell, E.A.; Shaw, D.E.; et al. Ensemble cryo-EM reveals conformational states of the nsp13 helicase in the SARS-CoV-2 helicase replication-transcription complex. *Nat. Struct. Mol. Biol.* **2022**, *29*, 250–260. [CrossRef] [PubMed]

89. Brant, A.C.; Tian, W.; Majerciak, V.; Yang, W.; Zheng, Z.M. SARS-CoV-2: From its discovery to genome structure, transcription, and replication. *Cell Biosci.* **2021**, *11*, 136. [CrossRef]

90. Long, S. SARS-CoV-2 Subgenomic RNAs: Characterization, Utility, and Perspectives. *Viruses* **2021**, *13*, 1923. [CrossRef]

91. Malone, B.; Campbell, E.A.; Darst, S.A. CoV-er all the bases: Structural perspectives of SARS-CoV-2 RNA synthesis. *Enzymes* **2021**, *49*, 1–37. [CrossRef]

92. Newman, J.A.; Douangamath, A.; Yadzani, S.; Yosaatmadja, Y.; Aimon, A.; Brandao-Neto, J.; Dunnett, L.; Gorrie-Stone, T.; Skyner, R.; Fearon, D.; et al. Structure, mechanism and crystallographic fragment screening of the SARS-CoV-2 NSP13 helicase. *Nat. Commun.* **2021**, *12*, 4848. [CrossRef]

93. Woo, P.C.; Lau, S.K.; Huang, Y.; Yuen, K.Y. Coronavirus diversity, phylogeny and interspecies jumping. *Exp. Biol. Med.* **2009**, *234*, 1117–1127. [CrossRef]

94. Robson, F.; Khan, K.S.; Le, T.K.; Paris, C.; Demirbag, S.; Barfuss, P.; Rocchi, P.; Ng, W.L. Coronavirus RNA Proofreading: Molecular Basis and Therapeutic Targeting. *Mol. Cell* **2020**, *79*, 710–727. [CrossRef] [PubMed]

95. Belshaw, R.; Pybus, O.G.; Rambaut, A. The evolution of genome compression and genomic novelty in RNA viruses. *Genome Res.* **2007**, *17*, 1496–1504. [CrossRef] [PubMed]

96. Gribble, J.; Stevens, L.J.; Agostini, M.L.; Anderson-Daniels, J.; Chappell, J.D.; Lu, X.; Pruijssers, A.J.; Routh, A.L.; Denison, M.R. The coronavirus proofreading exoribonuclease mediates extensive viral recombination. *PLoS Pathog.* **2021**, *17*, e1009226. [CrossRef]

97. Yan, L.; Yang, Y.; Li, M.; Zhang, Y.; Zheng, L.; Ge, J.; Huang, Y.C.; Liu, Z.; Wang, T.; Gao, S.; et al. Coupling of N7-methyltransferase and 3′-5′ exoribonuclease with SARS-CoV-2 polymerase reveals mechanisms for capping and proofreading. *Cell* **2021**, *184*, 3474–3485.e11. [CrossRef]

98. Dos Ramos, F.; Carrasco, M.; Doyle, T.; Brierley, I. Programmed-1 ribosomal frameshifting in the SARS coronavirus. *Biochem. Soc. Trans.* **2004**, *32*, 1081–1083. [CrossRef] [PubMed]

99. Thiel, V.; Ivanov, K.A.; Putics, A.; Hertzig, T.; Schelle, B.; Bayer, S.; Weissbrich, B.; Snijder, E.J.; Rabenau, H.; Doerr, H.W.; et al. Mechanisms and enzymes involved in SARS coronavirus genome expression. *J. Gen. Virol.* **2003**, *84*, 2305–2315. [CrossRef] [PubMed]

100. Nakagawa, K.; Lokugamage, K.G.; Makino, S. Viral and Cellular mRNA Translation in Coronavirus-Infected Cells. *Adv. Virus Res.* **2016**, *96*, 165–192. [CrossRef]

101. Kirchdoerfer, R.N.; Ward, A.B. Structure of the SARS-CoV nsp12 polymerase bound to nsp7 and nsp8 co-factors. *Nat. Commun.* **2019**, *10*, 2342. [CrossRef]

102. Saikrishnan, K.; Powell, B.; Cook, N.J.; Webb, M.R.; Wigley, D.B. Mechanistic basis of 5′-3′ translocation in SF1B helicases. *Cell* **2009**, *137*, 849–859. [CrossRef]

103. Singleton, M.R.; Dillingham, M.S.; Wigley, D.B. Structure and mechanism of helicases and nucleic acid translocases. *Annu. Rev. Biochem.* **2007**, *76*, 23–50. [CrossRef]

104. Mickolajczyk, K.J.; Shelton, P.M.M.; Grasso, M.; Cao, X.; Warrington, S.E.; Aher, A.; Liu, S.; Kapoor, T.M. Force-dependent stimulation of RNA unwinding by SARS-CoV-2 nsp13 helicase. *Biophys. J.* **2021**, *120*, 1020–1030. [CrossRef]

105. Jang, K.J.; Jeong, S.; Kang, D.Y.; Sp, N.; Yang, Y.M.; Kim, D.E. A high ATP concentration enhances the cooperative translocation of the SARS coronavirus helicase nsP13 in the unwinding of duplex RNA. *Sci. Rep.* **2020**, *10*, 4481. [CrossRef] [PubMed]

106. Sommers, J.A.; Loftus, L.N.; Jones, M.P., 3rd; Lee, R.A.; Haren, C.E.; Dumm, A.J.; Brosh, R.M., Jr. Biochemical analysis of SARS-CoV-2 Nsp13 helicase implicated in COVID-19 and factors that regulate its catalytic functions. *J. Biol. Chem.* **2023**, *299*, 102980. [CrossRef]

107. Shimberg, G.D.; Michalek, J.L.; Oluyadi, A.A.; Rodrigues, A.V.; Zucconi, B.E.; Neu, H.M.; Ghosh, S.; Sureschandra, K.; Wilson, G.M.; Stemmler, T.L.; et al. Cleavage and polyadenylation specificity factor 30: An RNA-binding zinc-finger protein with an unexpected 2Fe-2S cluster. *Proc. Natl. Acad. Sci. USA* **2016**, *113*, 4700–4705. [CrossRef] [PubMed]

108. Weiss, A.; Murdoch, C.C.; Edmonds, K.A.; Jordan, M.R.; Monteith, A.J.; Perera, Y.R.; Rodriguez Nassif, A.M.; Petoletti, A.M.; Beavers, W.N.; Munneke, M.J.; et al. Zn-regulated GTPase metalloprotein activator 1 modulates vertebrate zinc homeostasis. *Cell* **2022**, *185*, 2148–2163.e27. [CrossRef]

109. Maio, N.; Cherry, S.; Schultz, D.C.; Hurst, B.L.; Linehan, W.M.; Rouault, T.A. TEMPOL inhibits SARS-CoV-2 replication and development of lung disease in the Syrian hamster model. *iScience* **2022**, *25*, 105074. [CrossRef] [PubMed]

110. Ghosh, M.C.; Tong, W.H.; Zhang, D.; Ollivierre-Wilson, H.; Singh, A.; Krishna, M.C.; Mitchell, J.B.; Rouault, T.A. Tempol-mediated activation of latent iron regulatory protein activity prevents symptoms of neurodegenerative disease in IRP2 knockout mice. *Proc. Natl. Acad. Sci. USA* **2008**, *105*, 12028–12033. [PubMed]

111. Ghosh, M.C.; Zhang, D.L.; Ollivierre, H.; Eckhaus, M.A.; Rouault, T.A. Translational repression of HIF2alpha expression in mice with Chuvash polycythemia reverses polycythemia. *J. Clin. Investig.* **2018**, *128*, 1317–1325. [CrossRef]

112. Burns, G.S.; Thompson, A.J. Viral hepatitis B: Clinical and epidemiological characteristics. *Cold Spring Harb. Perspect. Med.* **2014**, *4*, a024935. [CrossRef]

113. Schollmeier, A.; Glitscher, M.; Hildt, E. Relevance of HBx for Hepatitis B Virus-Associated Pathogenesis. *Int. J. Mol. Sci.* **2023**, *24*, 4964. [CrossRef]

114. Brechot, C. Hepatitis B virus (HBV) and hepatocellular carcinoma. *J. Hepatol.* **1987**, *4*, 269–279. [CrossRef]

115. Wu, H.Y.; Guy, J.S.; Yoo, D.; Vlasak, R.; Urbach, E.; Brian, D.A. Common RNA replication signals exist among group 2 coronaviruses: Evidence for in vivo recombination between animal and human coronavirus molecules. *Virology* **2003**, *315*, 174–183. [CrossRef] [PubMed]

116. Eckhardt, S.G.; Milich, D.R.; McLachlan, A. Hepatitis B virus core antigen has two nuclear localization sequences in the Arginine-rich carboxyl terminus. *J. Virol.* **1991**, *65*, 575–582. [PubMed]

117. Tsukuda, S.; Watashi, K. Hepatitis B virus biology and life cycle. *Antivir. Res.* **2020**, *182*, 104925. [CrossRef] [PubMed]

118. Wei, L.; Ploss, A. Hepatitis B virus cccDNA is formed through distinct repair processes of each strand. *Nat. Commun.* **2021**, *12*, 1591. [CrossRef]

119. Dane, D.S.; Cameron, C.H. Virus-like particles in serum of patients with Australia-antigen associated hepatitis. *Lancet* **1970**, *295*, 649–698. [CrossRef]

120. van Hemert, F.J.; van de Klundert, M.A.; Lukashov, V.V.; Kootstra, N.A.; Berkhout, B.; Zaaijer, H.L. Protein X of hepatitis B virus: Origin and structure similarity with the central domain of DNA glycosylase. *PLoS ONE* **2011**, *6*, e23392. [CrossRef]

121. Ueda, C.; Langton, M.; Chen, J.; Pandelia, M.E. The HBx protein from Hepatitis B Virus coordinates a redox-active Fe-S cluster. *J. Biol. Chem.* **2022**, *298*, 101698. [CrossRef]

122. Gu, J.M.; Lim, S.O.; Oh, S.J.; Yoon, S.M.; Seong, J.K.; Jung, G. HBx modulates iron regulatory protein 1-mediated iron metabolism via reactive oxygen species. *Virus Res.* **2008**, *133*, 167–177. [CrossRef]

123. Bettany, A.J.; Eisenstein, R.S.; Munro, H.N. Mutagenesis of the iron-regulatory element further defines a role for RNA secondary structure in the regulation of ferritin and transferrin receptor expression. *J. Biol. Chem.* **1992**, *267*, 16531–16537. [CrossRef]

124. Aziz, N.; Munro, H.N. Iron regulates ferritin mRNA translation through a segment of its 5′ untranslated region. *Proc. Natl. Acad. Sci. USA* **1987**, *84*, 8478–8482. [CrossRef]

125. Rouault, T.A. The role of iron regulatory proteins in mammalian iron homeostasis and disease. *Nat. Chem. Biol.* **2006**, *2*, 406–414. [CrossRef] [PubMed]

126. Ramakrishnan, D.; Xing, W.; Beran, R.K.; Chemuru, S.; Rohrs, H.; Niedziela-Majka, A.; Marchand, B.; Mehra, U.; Zabransky, A.; Dolezal, M.; et al. Hepatitis B Virus X Protein Function Requires Zinc Binding. *J. Virol.* **2019**, *93*, e00250-19. [CrossRef] [PubMed]

127. Pritts, J.D.; Michel, S.L.J. Fe-S clusters masquerading as zinc finger proteins. *J. Inorg. Biochem.* **2022**, *230*, 111756. [CrossRef]

128. Beilschmidt, L.K.; Ollagnier de Choudens, S.; Fournier, M.; Sanakis, I.; Hograindleur, M.A.; Clemancey, M.; Blondin, G.; Schmucker, S.; Eisenmann, A.; Weiss, A.; et al. ISCA1 is essential for mitochondrial Fe(4)S(4) biogenesis in vivo. *Nat. Commun.* **2017**, *8*, 15124. [CrossRef] [PubMed]

129. Monttinen, H.A.M.; Bicep, C.; Williams, T.A.; Hirt, R.P. The genomes of nucleocytoplasmic large DNA viruses: Viral evolution writ large. *Microb. Genom.* **2021**, *7*, 649. [CrossRef]

130. Villalta, A.; Srour, B.; Lartigue, A.; Clemancey, M.; Byrne, D.; Chaspoul, F.; Loquet, A.; Guigliarelli, B.; Blondin, G.; Abergel, C.; et al. Evidence for [2Fe-2S](2+) and Linear [3Fe-4S](1+) Clusters in a Unique Family of Glycine/Cysteine-Rich Fe-S Proteins from Megavirinae Giant Viruses. *J. Am. Chem. Soc.* **2023**, *145*, 2733–2738. [CrossRef]

131. Zhang, B.; Bandyopadhyay, S.; Shakamuri, P.; Naik, S.G.; Huynh, B.H.; Couturier, J.; Rouhier, N.; Johnson, M.K. Monothiol glutaredoxins can bind linear $[Fe_3S_4]^+$ and $[Fe_4S_4]^{2+}$ clusters in addition to $[Fe_2S_2]^{2+}$ clusters: Spectroscopic characterization and functional implications. *J. Am. Chem. Soc.* **2013**, *135*, 15153–15164. [CrossRef]

132. Koonin, E.V.; Krupovic, M.; Agol, V.I. The Baltimore Classification of Viruses 50 Years Later: How Does It Stand in the Light of Virus Evolution? *Microbiol. Mol. Biol. Rev.* **2021**, *85*, e0005321. [CrossRef]

133. Peersen, O.B. A Comprehensive Superposition of Viral Polymerase Structures. *Viruses* **2019**, *11*, 745. [CrossRef]

134. de Farias, S.T.; Dos Santos Junior, A.P.; Rego, T.G.; Jose, M.V. Origin and Evolution of RNA-Dependent RNA Polymerase. *Front. Genet.* **2017**, *8*, 125. [CrossRef] [PubMed]

135. Menendez-Arias, L.; Sebastian-Martin, A.; Alvarez, M. Viral reverse transcriptases. *Virus Res.* **2017**, *234*, 153–176. [CrossRef] [PubMed]

136. Sessions, A.L.; Doughty, D.M.; Welander, P.V.; Summons, R.E.; Newman, D.K. The continuing puzzle of the great oxidation event. *Curr. Biol.* **2009**, *19*, R567–R574. [CrossRef]

137. Mahmoudabadi, G.; Milo, R.; Phillips, R. Energetic cost of building a virus. *Proc. Natl. Acad. Sci. USA* **2017**, *114*, E4324–E4333. [CrossRef]

138. Şimşek, B.; Özilgen, M.; Utku, F.Ş. How much energy is stored in SARS-CoV-2 and its structural elements? *Energy Storage* **2022**, *4*, e298. [CrossRef]

139. Sazanov, L.A. A giant molecular proton pump: Structure and mechanism of respiratory complex I. *Nat. Rev. Mol. Cell Biol.* **2015**, *16*, 375–388. [CrossRef]